J Geod (2013) 87:981–1001
DOI 10.1007/s00190-013-0662-z

ORIGINAL ARTICLE

Troposphere delays from space geodetic techniques, water vapor radiometers, and numerical weather models over a series of continuous VLBI campaigns

Kamil Teke · Tobias Nilsson · Johannes Böhm · Thomas Hobiger · Peter Steigenberger · Susana García-Espada · Rüdiger Haas · Pascal Willis

Received: 25 February 2013 / Accepted: 17 September 2013 / Published online: 10 October 2013

Abstract Continuous, very long baseline interferometry (VLBI) campaigns over 2 weeks have been carried out repeatedly, i.e., CONT02 in October 2002, CONT05 in September 2005, CONT08 in August 2008, and CONT11 in September 2011, to demonstrate the highest accuracy the current VLBI was capable at that time. In this study, we have compared zenith total delays (ZTD) and troposphere gradients as consistently estimated from the observations of VLBI, Global Navigation Satellite Systems (GNSS), and Doppler Orbitography and Radiopositioning Integrated by Satellite (DORIS) at VLBI sites participating in the CONT campaigns. We analyzed the CONT campaigns using the state-of-the-art software following common processing strategies as closely as possible. In parallel, ZTD and gradients were derived from numerical weather models, i.e., from the global European Centre for Medium-Range Weather Forecasts (ECMWF) analysis fields, the High Resolution Limited Area Model (European sites), the Japan Meteorological

Electronic supplementary material The online version of this article (doi:10.1007/s00190-013-0662-z) contains supplementary material, which is available to authorized users.

K. Teke (✉)
Department of Geomatics Engineering,
Hacettepe University, Ankara, Turkey
e-mail: kteke@hacettepe.edu.tr

K. Teke · J. Böhm
Department of Geodesy and Geoinformation,
Vienna University of Technology, Vienna, Austria
e-mail: johannes.boehm@tuwien.ac.at

T. Nilsson
Section 1.1, GPS/Galileo Earth Observations, GFZ German
Research Centre for Geosciences, Potsdam, Germany
e-mail: nilsson@gfz-potsdam.de

T. Hobiger
Space-Time Standards Group, National Institute
of Information and Communications Technology (NICT),
4-2-1 Nukui-Kitamachi, Koganei,
Tokyo 184-8795, Japan
e-mail: hobiger@nict.go.jp

P. Steigenberger
Institut für Astronomische und Physikalische Geodäsie,
Technische Universität München, Arcisstraße 21,
80333 Munich, Germany
e-mail: steigenberger@bv.tum.de

S. García-Espada · R. Haas
Department of Earth and Space Sciences,
Chalmers University of Technology,
Onsala Space Observatory, 43992 Onsala, Sweden
e-mail: rudiger.haas@chalmers.se

S. García-Espada
Instituto Geografico Nacional,
Apartado 148, 19080 Yebes, Spain
e-mail: s.gespada@oan.es

P. Willis
Institut national de l'information géographique et forestière,
Direction Technique, 73 avenue de Paris, Saint-Mandé,
94165, France
email: pascal.willis@ign.fr

P. Willis
Institut de Physique du Globe de Paris, Univ Paris Diderot,
Sorbonne Paris Cité, UMR 7154 CNRS,
75013 Paris, France

Agency-Operational Meso-Analysis Field (MANAL, over Japan), and the Cloud Resolving Storm Simulator (Tsukuba, Japan). Finally, zenith wet delays were estimated from the observations of water vapor radiometers (WVR) at sites where the WVR observables are available during the CONT sessions. The best ZTD agreement, interpreted as the smallest standard deviation, was found between GNSS and VLBI techniques to be about 5–6 mm at most of the co-located sites and CONT campaigns. We did not detect any significant improvement in the ZTD agreement between various techniques over time, except for DORIS and MANAL. On the other hand, the agreement and thus the accuracy of the troposphere parameters mainly depend on the amount of humidity in the atmosphere.

Keywords Troposphere delays · Space geodetic techniques · Numerical weather models · Water vapor radiometers

1 Introduction

Troposphere delays, strictly speaking delays in the neutral atmosphere, are an important error source for the measurements of space geodetic techniques. Validation and accuracy assessment of troposphere delays observed by various space geodetic techniques are essential before inter-technique combination studies of the Global Geodetic Observing System (GGOS, Rummel et al. 2005) of the International Association of Geodesy (IAG). Space geodetic techniques observing at microwave frequencies like very long baseline interferometry (VLBI), Global Navigation Satellite Systems (GNSS), and Doppler Orbitography and Radio Positioning Integrated by Satellite (DORIS) are affected by the same troposphere delays when considering the height differences at co-located sites, and a rigorous inter-technique combination should cover not only station coordinates, but also troposphere delays at the sites. Here, the co-located sites mean geodetic stations where equipment for several space geodetic techniques is installed. The distances between the antennas of space geodetic techniques at a co-located site usually do not exceed a few kilometers (see approximate horizontal distances between e.g., VLBI and GNSS antennas in Table 3).

Several studies on inter-technique comparisons of zenith total delays (ZTD) have been carried out to assess and validate the level of agreement between different techniques. For instance, Behrend et al. (2002) compared ZWD from a numerical weather prediction model, MM5, with those derived from VLBI, GPS, and water vapor radiometers (WVR) at three co-located sites in Europe (Madrid, Onsala, and Wettzell) in 1999 over six VLBI sessions. Steigenberger et al. (2007) presented standard deviations, biases, and correlations between GPS and VLBI ZWD estimates from homogeneously reprocessed GPS and VLBI observations of a global network over 11 years. Multi-technique comparisons of ZTD were carried out for the continuous VLBI campaigns CONT02 (Snajdrova et al. 2006) and CONT08 (Teke et al. 2011) using the data of GNSS, VLBI, DORIS, WVR, and NWM. Both studies indicate similar results in terms of biases and standard deviations between the techniques. They found larger standard deviations between ZTD series at low latitude sites. Ning et al. (2012) compared time series over 10 years of ZWD from the observations of GPS, VLBI, WVR, radiosondes and from the reanalysis product of European Centre for Medium-Range Weather Forecasts (ECMWF) at the Onsala site. They found that the standard deviations were less than 7 mm between GNSS, VLBI, and WVR, and that the best agreement was between VLBI and GNSS with a mean bias of −3.4 mm and a standard deviation of 5.1 mm. Bock et al. (2010) compared yearly biases and standard deviations of DORIS–GNSS ZTD differences from 2005 to 2008 at more than 30 co-located sites distributed over the globe. In addition to the above-mentioned studies, numerous assessments on the agreement of the troposphere parameters derived from a variety of spatial and temporal coverage of troposphere data from VLBI, GNSS, WVR, and numerical weather models were carried out, e.g., by Yang et al. (1999), Cucurull et al. (2000), Behrend et al. (2000), Gradinarsky et al. (2000), Niell et al. (2001), or Heinkelmann et al. (2011).

The main purpose of this paper is to investigate differences in the estimates of troposphere ZTD and gradients for the campaigns CONT02, CONT05, CONT08, and CONT11 as derived consistently by the space geodetic techniques, by NWM [European Centre for Medium-Range Weather Forecasts (ECMWF, global coverage), High Resolution Limited Area Model (HIRLAM, over Europe), Japan Meteorological Agency (JMA)-Operational Meso-Analysis Field (MANAL, over Japan) and Cloud Resolving Storm Simulator (CReSS, Tsukuba, Japan)] and by WVR. In particular, we focused on the agreement among CONT campaigns for each technique to see if an improvement of the agreement of ZTD and gradients could be achieved over time (over CONT campaigns), the site-specific (site-wise) distinctions of biases and standard deviations of ZTD differences during CONT campaigns, and the level of agreement of short-term troposphere delays from our results with long-term results derived from other comparison studies, e.g., by Steigenberger et al. (2007), Bock et al. (2010), and Ning et al. (2012). In Sect. 2 we present a summary of modeling troposphere delays for the analyses of space geodetic measurements. In Sect. 3 we describe the CONT campaigns and analysis options of each technique in detail. In Sect. 4, we introduce the data sets of the techniques and the troposphere ties due to the height differences between the antennas at each co-located site. In Sects. 4.3 and 4.4, we discuss the site-wise agreement of ZTD and of troposphere

north and east gradients derived from different techniques and for different CONT campaigns.

2 Modeling troposphere delays for the analyses of space geodetic measurements

The refractivity of the neutral part of the atmosphere (mainly in the troposphere) causes so-called troposphere delays on the microwave signals of space geodetic techniques. These delays can be calculated through numerical integration of the hydrostatic refractivity, $N_h(s)$, and the wet refractivity, $N_w(s)$, along the signal path, s, between the antenna, $H_{antenna}$, and the top of the neutral atmosphere, H_{trop}, with

$$\Delta L = 10^{-6} \int_{H_{antenna}}^{H_{trop}} [N_h(s) + N_w(s)]\, ds \quad (1)$$

e.g., by using ray-tracing algorithms (e.g., Böhm et al. 2006; Hobiger et al. 2008a, b; Urquhart et al. 2011; Nafisi et al. 2012) utilizing the fields of numerical weather models (NWM, e.g., HIRLAM: Undén et al. 2002; CReSS: Tsuboki and Sakakibara 2002; MANAL: Saito et al. 2006; ECMWF: Dee et al. 2011). Alternatively, troposphere delays can be estimated from WVR measurements (e.g., Elgered 1993) or from the measurements of space geodetic techniques. In the latter case, the troposphere delay, ΔL, can be divided into further parts and modeled in a linear form as follows (Davis et al. 1993):

$$\Delta L(\alpha, e) = \mathrm{ZHD} m_h(e) + \mathrm{ZWD} m_w(e) + m_g(e)[\mathrm{G_n}\cos(\alpha) + \mathrm{G_e}\sin(\alpha)]. \quad (2)$$

In Eq. (2), e denotes the outgoing vacuum elevation angle from the local horizon, α the horizontal angle from geodetic north (azimuth), ZWD the troposphere zenith wet delay, ZHD the zenith hydrostatic delay, $m_h(e)$ the troposphere hydrostatic mapping function, $m_w(e)$ the wet mapping function, $m_g(e)$ the gradient mapping function, and G_n and G_e are the so-called north and east total horizontal gradients, respectively. Since the hydrostatic delay changes slowly over time and is proportional to the density of air, ZHD can be calculated from total surface pressure and approximate coordinates of the station (e.g., Saastamoinen 1972; refined by Davis et al. 1985), assuming hydrostatic equilibrium. The accuracy of the ZHD calculated this way is in principle proportional to the accuracy of the surface pressure values with a pressure error of 1 hPa resulting in an error of 2.3 mm. On the other hand, the troposphere wet delay is the major error source in the observations of the space geodetic techniques due to the difficulties of modeling the rapidly varying wet refractivity in time and space. For most of the analyses of space geodetic techniques, ZHD are calculated from surface pressure measurements, mapped to the corresponding elevation angles of the observations with the hydrostatic mapping function, and reduced from each observation a priori to the parameter estimation. Then, ZWD and troposphere gradients are estimated from the observations of space geodetic techniques.

Un-modeled parts of the troposphere delay propagate to all geodetic estimates, especially to the TRF (e.g., Böhm and Schuh 2007; Steigenberger et al. 2009) and to the CRF (MacMillan and Ma 1997), in geodetic parameter estimation. Thus, it is important to model the troposphere delays as accurately as possible to estimate accurate geodetic and geodynamic parameters from space geodetic measurements. This has been investigated in several studies, e.g., Herring (1986), Davis et al. (1991), Bevis et al. (1992), MacMillan and Ma (1994), Tesmer et al. (2007), and Steigenberger et al. (2007).

3 Co-located sites during CONT campaigns, techniques, and analysis options

Approximately, every third year the International VLBI Service for Geodesy and Astrometry (IVS, Schuh and Behrend 2012) has carried out continuous VLBI campaigns over 2 weeks to demonstrate the highest accuracy of the VLBI system at that time. In this paper, we compare troposphere ZTD and gradients derived in the last four CONT campaigns (CONT02 from 16 to 31 October 2002, CONT05 from 12 to 27 September 2005, CONT08 from 12 to 27 August 2008, and CONT11 from 15 to 30 September 2011). The co-located sites in these campaigns are shown in Fig. 1.

Sites that contributed to all four CONT campaigns are Ny-Ålesund (Svalbard/Norway), Onsala (Sweden), Wettzell

Fig. 1 VLBI co-located sites during CONT campaigns. *Red circles* illustrate the sites that contributed to all CONT campaigns. The sites shown as *blue* and *green circles* were involved in three CONT campaigns and less than three CONT campaigns, respectively

Table 1 Geodetic instruments at co-located sites during CONT campaigns. The headers of the columns (02, 05, 08, and 11) denote CONT02, CONT05, CONT08, and CONT11

Co-located sites	Country	Lat. (°)	Lon. (°)	Sites contributing to CONT campaigns				VLBI acronym	IGS acronym	IDS acronym
				02	05	08	11			
Ny-Ålesund	Norway	78.93	11.87	+	+	+	+	NYALES20	NYA1	spib, spjb
Gilmore Creek	USA	64.98	212.50	+	+			GILCREEK	FAIR	–
Svetloe	Russia	60.53	29.78		+	+		SVETLOE	SVTL	–
Onsala	Sweden	57.39	11.93	+	+	+	+	ONSALA60	ONSA	–
Badary	Russia	51.77	102.23				+	BADARY	BADG	badb
Wettzell	Germany	49.14	12.88	+	+	+	+	WETTZELL	WTZR	–
Algonquin Park	Canada	45.95	281.93	+	+			ALGOPARK	ALGO	–
Medicina	Italy	44.52	11.65			+		MEDICINA	MEDI	–
Zelenchukskaya	Russia	43.79	41.57			+	+	ZELENCHK	ZECK	–
Westford	USA	42.61	288.51	+	+	+	+	WESTFORD	WES2	–
Yebes	Spain	40.52	356.91				+	YEBES40M	YEBE	–
Tsukuba	Japan	36.10	140.09		+	+	+	TSUKUB32	TSKB	–
Kokee Park	USA	22.13	200.33	+	+	+	+	KOKEE	KOKB	koka, kolb
Fortaleza	Brazil	−3.88	321.57				+	FORTLEZA	BRFT	–
Hartebeesthoek	South Africa	−25.89	27.69	+	+	+	+	HARTRAO	HRAO	hbkb, hbmb
TIGO Concepcion	Chile	−36.84	286.97		+	+	+	TIGOCONC	CONZ	–
Hobart	Australia	−42.81	147.44				+	HOBART12	HOB2	–

(Germany), Westford (USA), Kokee Park (Hawaii, USA), and Hartebeesthoek (South Africa), whereas Tsukuba (Japan) and TIGO Concepcion (Chile) were involved in three campaigns (CONT05, CONT08, and CONT11). The GNSS antennas and DORIS beacons co-located with the VLBI antennas are listed in Table 1. Note that in all tables the names of the co-located sites are ordered according to the latitude of the sites from north to south.

The availability of troposphere parameters from the various techniques at the co-located sites is summarized in Table 2. Troposphere estimates from GNSS are available for all CONT02 and CONT05 sites, whereas we do not have troposphere results at ZECK (Zelenchukskaya in Russia) during CONT08 or at BADG (Badary, Russia) during CONT11. The DORIS beacons which contributed to CONT02, CONT05, CONT08, and CONT11 campaigns were hbkb and hbmb at Hartebeesthoek (hbkb during CONT02 and CONT05, hbmb during CONT08 and CONT11), koka and kolb at Kokee Park (koka during CONT02, kolb during CONT05, CONT08, CONT11), spib and spjb at Ny-Ålesund (spib during CONT02, spjb during CONT05, CONT08, CONT11), and badb at the co-located site Badary (only CONT11). Note that four-letter IDS acronyms of the DORIS beacons are written in lowercase and the IGS acronyms of the GNSS antennas in uppercase as an easy convention to distinguish DORIS and GNSS stations. Concerning NWM, we calculated ZTD and gradients from fields of the ECMWF for all CONT campaigns at all co-located sites, MANAL at Tsukuba during CONT05 and CONT11, and CReSS at Tsukuba during CONT08. ZTD from HIRLAM were made available at Onsala and Wettzell for all CONT campaigns. The other sites in Europe where HIRLAM data were used to determine troposphere parameters are shown in Table 2.

We calculated tide-free ellipsoidal heights of the antenna reference points (ARP) of VLBI, GNSS, and DORIS antennas from ITRF2008 (Altamimi et al. 2011) coordinates. The WVR heights (see Table 3) were provided from various local measurements at the stations and may not be as reliable, but they are accurate enough for our study. The height differences between the ARP and a reference height were needed for the calculation of reliable and accurate troposphere ties (see Sect. 4.1). In this study we selected the VLBI ARP heights as the reference height at each VLBI co-located site. This is mainly due to the fact that VLBI data are available for all stations and all campaigns, and also due to the better stability of the VLBI antennas over time compared to those of GNSS and DORIS where there are more frequent equipment changes. We provided ARP heights of GNSS antennas by adding the ARP up (radial) eccentricities to the geodetic marker heights. These eccentricities are usually only a few cm, although the eccentricity at Onsala is 1 m; see Table 3. It should be noted that the horizontal distances between DORIS

Table 2 Availability of troposphere parameters at co-located sites

Co-located sites	VLBI				GNSS				DORIS				HIRLAM				WVR			
	02	05	08	11	02	05	08	11	02	05	08	11	02	05	08	11	02	05	08	11
Ny-Ålesund	+	+	+	+	+	+	+	+	+	+	+	+				+				
Gilmore Creek	+	+				+														
Svetloe		+	+			+	+								+					
Onsala	+	+	+	+	+	+	+	+					+	+	+	+	+	+	+	+
Badary				+								+								
Wettzell	+	+	+	+	+	+	+	+					+	+	+	+	+	+	+	
Algonquin Park	+	+			+	+												+		
Medicina			+				+								+					
Zelenchukskaya			+	+				+								+				
Westford	+	+	+	+	+	+	+	+												
Yebes				+																
Tsukuba		+	+	+		+	+	+										+	+	+
Kokee Park	+	+	+	+	+	+	+	+	+	+	+	+					+	+		
Fortaleza				+				+												
Hartebeesthoek	+	+	+	+	+	+	+	+	+	+	+	+						+		
TIGO Concepcion		+	+	+		+	+	+												
Hobart				+				+												

Troposphere parameters from the ECMWF were derived at all co-located sites. MANAL data are available at Tsukuba for CONT05 and CONT11 and CReSS data at Tsukuba for CONT08. The headers of the columns (02, 05, 08, and 11) denote CONT02, CONT05, CONT08, and CONT11

Table 3 ITRF2008 ellipsoidal heights and approximate horizontal distances of the co-located VLBI, GNSS, and DORIS antennas, and WVR involved in CONT campaigns

Co-located sites	VLBI height (m)	GNSS antenna phase center height (m) [reference point height + up eccentricity[b]]	DORIS height (m)	WVR height (m)	VLBI-GNSS approximate horizontal distance (m)	VLBI-DORIS approximate horizontal distance (m)
Ny-Ålesund	87.79	84.70 + 0.00	53.06 (spjb)	–	106	1,475
Gilmore Creek	332.53	319.44 + 0.09	–	–	93	–
Svetloe	86.47	77.12 + 0.03	–	–	82	–
Onsala	59.73	46.02 + 1.00	–	∼47[c]	79	–
Badary	822.05	–	812.95 (badb)	–	–	92
Wettzell	669.56	666.46 + 0.07	–	∼666	139	–
Algonquin Park	224.45	201.34 + 0.10	–	∼201	111	–
Medicina	67.60	50.45 + 0.00	–	–	60	–
Zelenchukskaya	1,175.48	1,166.71 + 0.05	–	–	65	–
Westford	87.19	85.44 + 0.00	–	–	58	–
Yebes	989.40[a]	–	–	–	–	–
Tsukuba	85.14	67.67 + 0.00	–	∼64[c]	303	–
Kokee Park	1,177.00	1,167.76 + 0.06	1,167.38 (kolb)	∼1,167	45	398
Fortaleza	23.48	22.06 + 0.01	–	–	–	–
Hartebeesthoek	1,416.12	1,414.56 + 0.08	1,560.01 (hbmb)	∼1,410	164	2,235
TIGO Concepcion	171.37	181.10 + 0.09	–	–	120	–
Hobart	41.14[a]	41.48 + 0.00	–	–	108	–

[a]Heights are estimated from CONT11 because they are not available in ITRF2008
[b]GNSS antenna reference point eccentricities are provided in the station log files at the IGS web site (http://igscb.jpl.nasa.gov)
[c]WVR at Onsala is Astrid and at Tsukuba is WVR28 (see Sect. 3.2)

and VLBI stations at co-located sites are quite large. At Ny-Ålesund the distance is about 1,475 m, at Kokee Park 398 m, and at Hartebeesthoek 2,235 m. This will eventually degrade the agreement of ZTD between DORIS and other techniques (Bock et al. 2010). The horizontal distances between VLBI and GNSS antennas are smaller, between 45 m at Kokee Park (KOKB) and 303 m at Tsukuba (TSKB) (see Table 3).

3.1 Space geodetic solutions

To ensure reliable comparisons, similar models were used for the analyses of space geodetic observations (see Sects. 3.1.1, 3.1.2, and 3.1.3). Additionally, we aimed at consistent estimation intervals and epochs of ZTD and gradients across all techniques. Whenever possible, ZTD were estimated (strictly speaking, ZWD are estimated in addition to a priori ZHD) at every integer hour and troposphere gradients every 6 h (see Table 6).

3.1.1 Very long baseline interferometry (VLBI)

We analyzed the VLBI observations during CONT campaigns with the Vienna VLBI Software (VieVS, Böhm et al. 2012), which is developed at the Department of Geodesy and Geoinformation at the Vienna University of Technology. We did not remove observations below a certain elevation angle, nor did we down-weight observations at low elevation angles. The IVS usually schedules observations down to 5°. Source coordinates were fixed to ICRF2 (International Celestial Reference Frame 2, Fey et al. 2009) except for sources not in the ICRF2 catalogue, which were estimated. The IERS C04 08 series (Bizouard and Gambis 2009) was used for a priori values of Earth orientation parameters (EOP), and high-frequency EOP variations were modeled as recommended by the IERS Conventions 2010 (Petit and Luzum 2010). Constant EOP residuals were estimated once per 24 h VLBI session. Tidal and non-tidal atmospheric loading (Petrov and Boy 2004), as well as tidal ocean loading corrections based on the ocean model FES2004 (Lyard et al. 2006), were introduced for each observation prior to the adjustment. Troposphere ZHD were computed using surface pressure values recorded at the sites (Saastamoinen 1972; Davis et al. 1985) and mapped down with the hydrostatic Vienna Mapping Functions 1 (VMF1, Böhm et al. 2006). Daily no-net-translation (NNT) and no-net-rotation (NNR) conditions were imposed on the estimated antenna coordinates relative to the a priori coordinates from the ITRF2008 catalogue (Altamimi et al. 2011). Antennas not available in ITRF2008 were excluded from the datum. ZWD and total gradients were estimated as hourly and 6-hourly piece-wise linear offsets. We used VMF1 and the gradient mapping function as introduced by Chen and Herring (1997).

3.1.2 Global Navigation Satellite Systems (GNSS)

The GNSS solutions are based on the 2011 reprocessing effort of the Center for Orbit Determination in Europe (CODE, Dach et al. 2009) which is documented in Dach et al (2012). In contrast to the CODE contribution to the IGS reprocessing campaign (Steigenberger et al. 2011), this reprocessing is based on the IGS08 reference frame and the igs08.atx antenna model (Rebischung et al. 2012) and is consistent with the IERS Conventions 2010. GNSS observation data of a global network of 80–250 stations were processed with the current development version 5.1 of the Bernese GPS Software (Dach et al. 2007). The CONT02 results are based on GPS data only, whereas the other CONT campaigns are processed in a rigorous GPS/GLONASS combination. GPS/GLONASS satellite orbits, Earth rotation parameters, station coordinates, and troposphere ZWD and gradients are estimated in one common adjustment. A detailed description of the estimated parameters and applied models is available at ftp://ftp.unibe.ch/aiub/REPRO_2011/CODE_REPRO_2011.ACN.

Cumulative solutions for each CONT campaign were computed solving for one set of station coordinates for all stations and continuous piece-wise linear troposphere parameters for the GNSS stations co-located to VLBI stations of the CONT campaigns. The datum was defined with NNR conditions of the IGS08 fiducial sites w.r.t. IGS08. A cut-off angle of 5° and elevation-dependent observation weighting with $w = 1/\cos^2 z$, where z is the zenith angle, were applied. A priori ZHD were interpolated from the ECMWF values provided, while VMF1 was used as the mapping function. ZWD and gradients were estimated as piece-wise linear function with a temporal resolution of 1 and 6 h, respectively. In contrast to the default setup for the CODE reprocessing, atmospheric pressure loading was applied on the observation level with the model of Wijaya et al. (2013). To be consistent, the S1/S2 tidal atmospheric corrections were used from the same model.

3.1.3 Doppler Orbitography and Radiopositioning Integrated by Satellite (DORIS)

The DORIS observations during the CONT campaigns were analyzed with the GIPSY-OASIS II software package from Jet Propulsion Laboratory, Pasadena, USA. We tuned our regular processing strategy used at IGN to provide operational geodetic results: ignwd08 as documented in Willis et al. (2010b), using in particular refined processing strategies for handling solar radiation pressure (Gobinddass et al. 2009) and atmospheric drag (Gobinddass et al. 2010). To be more consistent with the other techniques, we lowered our elevation cutoff from 10° to 5° without using any down-weighting of the observations at lower elevation. Station coordinates

were fixed to an internal reference (tf_110726a), aligned on ITRF2008 (Altamimi et al. 2011), but using more recent DORIS data (Willis et al. 2012b). No discontinuities were found in the coordinate time series for these stations (Willis et al. 2009). Bulletin A was used as a priori for the Earth orientation parameters, which were also estimated in the DORIS runs once per day. No atmospheric loading correction was used, but ocean loading corrections were introduced using the FES2004 model. VMF1 was used as troposphere mapping function. Total horizontal gradients (2 parameters) were estimated once a day, following early tests recently done (Willis et al. 2012a). More information about the DORIS analysis is described by Willis et al. (2010b, 2012b).

3.2 Water vapor radiometer (WVR)

A water vapor radiometer (WVR) makes measurements of the thermal radiation from the sky at microwave frequencies. From these measurements, the wet delay can be inferred (Elgered 1993). Typically, two frequencies are used (normally, one around 20 GHz and one around 30 GHz) to be able to separate the contributions from water vapor and liquid water in clouds. Nevertheless, for several reasons the WVR measurements are unreliable during rain. Furthermore, careful calibration of the radiometers is needed, and the conversion factor between the brightness temperatures measured by the WVR and the wet delay must be known precisely.

During the CONT campaigns, several stations operated one or more WVR, especially during CONT05. At Onsala the two radiometers Astrid (Elgered and Jarlemark 1998) and Konrad (Stoew and Rieck 1999) were operated in all of the campaigns. In this study, we used the data from Astrid WVR. At Hartebeesthoek, a WVR from ETH Zürich was operated during CONT05, while Radiometric radiometers were operated at Wettzell (CONT02, CONT05, and CONT08), Tsukuba (CONT05, CONT08, and CONT11), Kokee Park (CONT02 and CONT05), and Algopark (CONT05) (see co-located techniques with WVR at co-located sites of CONT campaigns in Table 2). The way the conversion factor between brightness temperature and wet delay was obtained was different for different stations. For example, at Tsukuba this factor was obtained by a fit of the measured brightness temperatures to radiosonde data (however, not necessarily for the exact period of the CONT campaigns). For the Onsala radiometers, the procedure is described by Jarlemark (1997).

Most radiometers were operated in the so-called sky mapping mode, meaning that the WVR moved around making measurements in many different directions covering the whole sky (above 20° elevation angle) quite well. From the slant wet delays measured by these, we estimated the ZWD and the wet gradients in a least squares adjustment. The ZWD and gradients for this study were modelled as piece-wise linear functions in 1 h and 6 h intervals, respectively. Some radiometers, however, observed only in the zenith direction (Tsukuba, Algonquin Park); hence, the measurements were insensitive to the horizontal gradients. Thus, for those WVR we estimated only the ZWD.

3.3 Numerical Weather Models (NWM)

3.3.1 European Centre for Medium-Range Weather Forecasts (ECMWF)

We used 6-hourly operational pressure levels analysis data of the ECMWF to determine ZHD and ZWD above the sites by vertical integration, requiring inter- or extrapolation to the site height depending on whether the site was above or below the lowest (1,000 hPa) level. Profiles around the sites were downloaded with a horizontal grid spacing of 0.25°, and the closest profile was utilized. For the determination of the gradients, the two adjacent profiles were taken in north–south and east–west direction to calculate north and east gradients, respectively, following an approach described by Böhm and Schuh (2007). All troposphere parameters derived from the ECMWF are made available at http://ggosatm.hg.tuwien.ac.at.

3.3.2 Cloud Resolving Storm Simulator (CReSS)

The CReSS is a non-hydrostatic model which allows resolving clouds and other small structures with the purpose of simulating meteorological phenomena ranging from cloud to mesoscale size (Tsuboki and Sakakibara 2002). This model is expected to provide accurate information about the spatial and temporal distribution of wet refractivity fields during extreme weather situations. However, CReSS relies on well-selected boundary conditions and other driving parameters to achieve model output, which reflects the true weather conditions well. The National Research Institute for Earth Science and Disaster Prevention (NIED) in Japan has set up this model on a 200×240 km area around Tokyo on a routine basis. NIED runs the CReSS as a forecast model, which is initialized every 24 h at 0 UT (Universal Time), providing output for every hour of the day. The grid spacing of this dedicated model is one kilometer, with a vertical extent up to 15 km and 45 height levels. Thus, when utilizing such models for ray tracing, one has to face the problem that the propagation path lies only partly within the model and soon leaves the area which is covered by the model, either by crossing the uppermost height level or by escaping laterally. Therefore, it is necessary to embed the fine-mesh model inside a coarser grid NWM (JMA, see Sect. 3.3.3 and Hobiger et al. 2010).

Table 4 HIRLAM data for the European VLBI stations that contributed to CONT campaigns as provided by both the Meteorological Spanish (AEMET) and Swedish (SMHI) agencies

Co-located sites	CONT02	CONT05	CONT08	CONT11
Ny-Ålesund	–	–	–	C (11 × 11) SMHI
Svetloe	–	–	G (5 × 5) SMHI	–
Onsala	A (50 × 50) AEMET	A (50 × 50) AEMET	G (5 × 5) SMHI	G (5 × 5) SMHI
Wettzell	B (20 × 20) AEMET	B (20 × 20) AEMET	E (11 × 11) SMHI	C (11 × 11) SMHI
Medicina	–	–	G (5 × 5) AEMET	–
Zelenchukskaya	–	–	–	C (11 × 11) SMHI

The sizes of grids are in km

3.3.3 Japan Meteorological Agency (JMA)-Operational Mesoscale Analysis Fields (MANAL)

The MANAL (Saito et al. 2006) data sets obtained from the JMA offer a good trade-off between the time resolution and the area covered by the model. As analysis models are generated every 3 h and the horizontal grid spacing is approximately 10 km (changed on April 7, 2009, providing a 5 km spacing instead of the 10 km grid), the MANAL data sets are a suitable choice for modelling atmospheric path delays in the East Asia region and are routinely used for ray-tracing processing with Kashima Ray-Tracing Tools (KARAT, Hobiger et al. 2008a).

3.3.4 High Resolution Limited Area Model (HIRLAM)

HIRLAM is a numerical weather model for short-range forecasting that is used by several European national meteorological services (Undén et al. 2002). It is a limited area forecasting model that uses ECMWF as boundary conditions. Different grid spacings are available, horizontally from 50 to 5 km, and vertically between 16 and 60 levels. The temporal resolution is 6 h in analysis mode, and predictions are available, e.g., with 3 and 6 h resolution. Depending on the size of the coverage area and the horizontal grid spacing, the different HIRLAM grids can be classified using a letter and a number, where the letter (A, B, C, F, G and E) denotes the coverage area and the number denotes the horizontal grid spacing in km (from 50 to 5). HIRLAM data were provided from both the Spanish Meteorological Agency, Agencia Estatal de Meteorología (AEMet), and the Swedish Meteorological and Hydrological Institute (SMHI). As different HIRLAM data coverage (A50, B20, C22, C11, E11, F16 and G05) are available for the European VLBI sites, Table 4 shows the chosen HIRLAM data grid spacing for each European station for each CONT campaign. The criterion used to select among the different spacings is to have the smallest grid spacing available for a particular site (i.e., G05 spacing is preferred when it is available for the site and the time span).

We used HIRLAM files with their corresponding grid spacing and vertical levels, and combined analysis and forecast data to achieve a temporal resolution of 3 h. This was done by adjusting the 3 h forecast data by corrections based on a comparison of the 6 h forecast data with the corresponding analysis data. So-called hybrid-level data of humidity and temperature together with surface pressure and geopotential data were extracted for the four nearest grid points around each station for each 6 h epoch during each CONT campaign. Based on these data, we calculated the vertical profiles of pressure, temperature, and humidity for each station. Finally, we used vertical integration to calculate the ZWD and we used surface pressure from the HIRLAM model to calculate ZHD.

4 Data analysis

We applied basic descriptive statistics to assess the agreement between the various estimates of ZTD and gradients. We calculated the biases and standard deviations of the differences of ZTD and gradients as well as the Pearson correlation coefficients (shared variances between two data sets) between each pair of series. To decide on the statistical significance of the correlation coefficients, we considered p values with a critical value of 0.05. The p value is the probability of making a false detection when determining if two data sets are correlated (Schervish 1996). We did not remove outliers from the differences of ZTD and gradients. This was done mainly to reveal the agreement between the techniques objectively without causing any artifacts based on the chosen criteria of outlier elimination. However, the techniques were free to optimize in terms of their analysis options, e.g., treating outlier observations within their analyses. We basically focused on comparing the site-wise agreement between ZTD and gradients from different CONT campaigns to figure out if any observational accuracy improvement occurred over time.

4.1 Troposphere ties

We define troposphere hydrostatic and wet ties as the corrections to ZHD and ZWD estimates of a technique at an estimation epoch due to the differential delay between the technique's antenna reference point and the reference height at a co-located site. In Table 5, the height differences and

Table 5 Height differences and mean troposphere ties of the co-located VLBI, GNSS, and DORIS stations, and the WVR involved in CONT11

Co-located site	VLBI-GNSS height difference (m)	Mean GNSS troposphere ties ZTD = ZHD + ZWD (mm)	VLBI-DORIS height difference (m)	Mean DORIS troposphere ties ZTD = ZHD + ZWD (mm)	VLBI-WVR height difference (m)	Mean WVR troposphere ties ZTD = ZHD + ZWD (mm)
Ny-Ålesund	3.10	$-0.96 = -0.87 + (-0.09)$	34.73	$-10.75 = -9.79 + (-0.97)$	–	–
Onsala	12.71	$-4.15 = -3.49 + (-0.66)$	–	–	∼13	$-0.68 = 0.00 + (-0.68)$
Badary	–	–	9.10	$-2.50 = -2.30 + (-0.20)$	–	–
Wettzell	3.03	$-0.91 = -0.78 + (-0.13)$	–	–	–	–
Westford	1.75	$-0.58 = -0.47 + (-0.11)$	–	–	–	–
Tsukuba	17.47	$-5.89 = -4.65 + (-1.24)$	–	–	∼21	$-1.43 = 0.00 + (-1.43)$
Kokee Park	9.18	$-2.69 = -2.20 + (-0.49)$	9.62	$-2.82 = -2.30 + (-0.52)$	–	–
Fortaleza	1.41	$-0.47 = -0.37 + (-0.10)$	–	–	–	–
Hartebeesthoek	1.47	$-0.38 = -0.34 + (-0.04)$	−143.90	$36.37 = 32.94 + (3.43)$	–	–
TIGO Concepcion	−9.82	$3.09 = 2.69 + 0.40$	–	–	–	–
Hobart	−0.35	$0.11 = 0.10 + 0.01$	–	–	–	–

mean troposphere ties for CONT11 for the GNSS, DORIS, and WVR stations w.r.t. VLBI are shown. For this study we computed troposphere hydrostatic and wet ties (ΔZHD and ΔZWD) from the analytical equations of Brunner and Rüeger (1992) based on the height differences and 6 hourly ECMWF data of water vapor pressure, total pressure, and temperature (Teke et al. 2011) as shown in Eqs. (3)–(5)

$$p = p_0 \left(1 - \frac{\gamma(H - H_0)}{T_0}\right)^{\frac{g}{\gamma R_L}}, \tag{3}$$

$$\Delta\mathrm{ZHD} = \frac{0.0022768(p - p_0)}{1 - 0.00266\cos(2\phi_0) - 0.28 \times 10^{-6} H_0}, \tag{4}$$

$$\Delta\mathrm{ZWD} = \frac{-2.789 e_0}{T_0^2}\left(\frac{5{,}383}{T_0} - 0.7803\right)\gamma(H - H_0), \tag{5}$$

where H_0 denotes the height of the VLBI antenna reference point. The parameters e_0, p_0, and T_0 are the water vapor pressure, total pressure, and temperature at the reference height; H and p are the height and total pressure at the co-located site, γ denotes the average temperature lapse rate, g is the gravity at the site, and R_L the specific gas constant. All the meteorological quantities mentioned above were interpolated to the ZTD estimation epochs. Then, time-dependent (epoch-wise) troposphere ties were calculated and reduced from each ZTD estimate before comparisons. In the case of WVR, only wet troposphere ties were considered because the ZHD were calculated from the pressure recordings at the VLBI antennas to get ZTD for WVR, which means that ZHD for WVR were provided already at the reference height of the co-located site. This is the reason that the hydrostatic ties of WVR are zero in Table 5.

For instance, the mean troposphere tie of the DORIS beacon hbmb at Hartebeesthoek was derived as 36.4 mm ($h_{\mathrm{DORIS}} - h_{\mathrm{VLBI}} = 143.9$ m) (see Table 5). After adding the troposphere ties at each epoch to the DORIS ZTD estimates, the mean bias between VLBI and DORIS was reduced from 40.6 to 4.3 mm (see supplementary material for this and more examples). The epoch-wise troposphere ties during CONT11 between the DORIS antenna (hbmb) and the reference height (VLBI ARP height) at the co-located site Hartebeesthoek are plotted in Fig. 2 to show the variability of total troposphere ties during a period of 15 days.

In Fig. 2, the hydrostatic ties vary by 2 mm which is mainly caused by the atmospheric tides. After adding the wet ties, the dispersion of total ties extends to 7 mm, which is due to the large height differences between the antennas and large humidity variations at Hartebeesthoek. Readers are referred to the supplementary files of this paper to see the plots of hydrostatic and total troposphere ties of the GNSS antennas, DORIS beacons, and WVR (only wet ties) w.r.t. the VLBI reference heights during the CONT campaigns. Due to the rapid and large changes of the troposphere wet ties

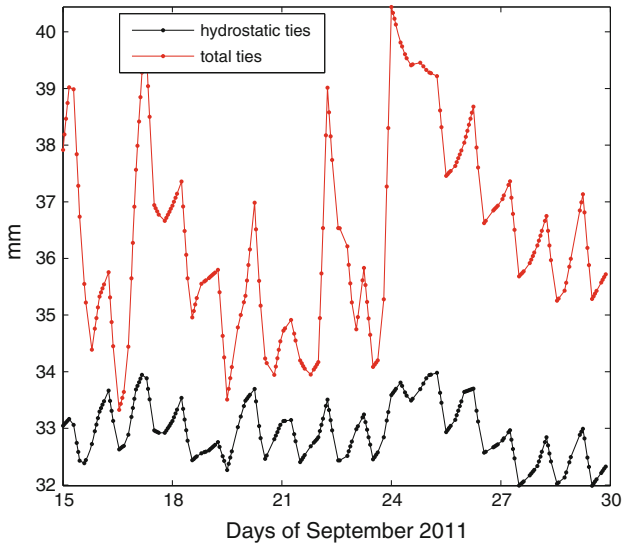

Fig. 2 Troposphere ties during the CONT11 campaign between the DORIS beacon (hbmb, height 1,560.0 m) and the reference height (VLBI ARP height 1,412.1 m) at the co-located site Hartebeesthoek. *Red* and *black lines* illustrate total and hydrostatic ties, respectively

over short time intervals, we strongly recommend adding the troposphere ties to ZTD at each estimation epoch instead of introducing a mean per CONT campaign. This will lead to a more rigorous comparison between ZTD derived from the different techniques.

4.2 Data types for comparisons

For the comparisons we used ZTD from WVR, from the space geodetic techniques GNSS, VLBI, and DORIS, and from the numerical weather models ECMWF, MANAL, CReSS, and HIRLAM. In Table 6 the types of the estimates and estimation intervals for the techniques are shown with the important parameterization for the estimation of troposphere delays in the analyses of space geodetic observations, i.e., troposphere mapping function, elevation cutoff angle, and if elevation angle-dependent down-weighting was introduced for the data analyses. It is worth emphasizing that all gradients from the techniques except WVR (wet gradients only) are total gradients.

The ZTD and gradients were provided for all techniques at UT integer hours, except for ZTD from DORIS. Thus, we interpolated linearly the DORIS ZTD to UT integer hours except for gaps longer than 1 hour. The distribution of the ZTD epochs from DORIS depends on the observations during the satellite passes, and the accuracies are most probably related to observed satellite constellations (see Table 7).

DORIS observations contain gaps since there is not always a DORIS satellite in view. For instance, each day from 2 to 7 UT and 15 to 19 UT during CONT08 at the DORIS beacon kolb, ZTD estimates were not avail-

Table 6 The optimized parameterization used in the analyses of the space geodetic techniques for the troposphere estimation are given in the second, third, and fourth columns. The types and intervals of the troposphere data available for the comparisons are given in columns five to seven

Technique	Troposphere mapping function	Elevation cut-off angle (°)	If down-weighting to observations introduced	Zenith wet/total delay	Estimation interval of zenith delay	Estimation interval of gradients
VLBI	VMF1	5	No	ZWD, ZTD	1 h	6 h (total gradients)
GNSS	VMF1	5	Yes	ZWD, ZTD	1 h	6 h (total gradients)
DORIS	VMF1	5	No	ZTD	Per satellite pass	1 day (total gradients)
WVR	$1/\sin(e^*)$	20	No	ZWD	1 h	6 h (wet gradients)
ECMWF	–	–	–	ZWD, ZTD	6 h	6 h (total gradients)
CReSS	–	–	–	ZWD, ZTD	1 h (CONT08)	1 h (total gradients) (CONT08)
MANAL	-	-	-	ZWD, ZTD	6 h (CONT05)	6 h (total gradients) (CONT05)
					3 h (CONT11)	3 h (total gradients) (CONT11)
HIRLAM	–	–	–	ZWD, ZTD	2 h	–

e^* denotes the elevation angle of the observation

Table 7 Satellite constellations observed by DORIS during CONT campaigns

	CONT02	CONT05	CONT08	CONT11
Envisat	✓	✓	✓	✓
Spot2	✓	✓	✓	✓
Spot4	✓	✓	✓	✓
Spot5	✓	✓	✓	✓
Topex	✓	–	–	–
Cryosat2	–	–	–	✓
Jason2	–	–	✓	✓

able. Thus, we did not interpolate ZTD from DORIS within these gaps which are longer than 1 h. The interpolation of DORIS ZTD to UT integer hours might cause some artifacts and a degraded agreement of DORIS ZTD with those derived from other techniques (Bock et al. 2010). Interpolating the troposphere parameters from the other techniques to the epochs when DORIS estimates are available would have yielded a slightly better agreement of the DORIS estimates.

For the comparison, we considered only common epochs of ZTD and gradients between two techniques after removing the troposphere ties per epoch (see the Eqs. (3)–(5) in Sect. 4.1 for the calculation of troposphere ties). For example, during each CONT campaign the number of common ZTD epochs per station is about 360 between GNSS and VLBI and about 60 between GNSS and ECMWF. The numbers of common epochs between each pair of techniques at each co-located site during the CONT campaigns is provided in the supplementary material.

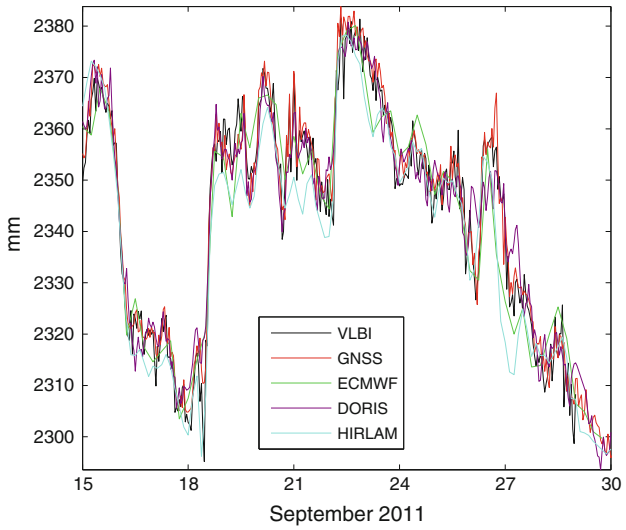

Fig. 3 ZTD at the co-located site Ny-Ålesund during CONT11. The GNSS and the DORIS antenna are NYA1 and spjb, respectively

4.3 Inter-technique comparisons of ZTD

In this section, we present the results of inter-technique comparisons of ZTD derived from different space geodetic techniques and numerical weather models to assess the level of agreement. For example, Fig. 3 shows the ZTD series derived from different techniques at Ny-Ålesund. In this section, we mainly discuss the site-wise mean biases and standard deviations of ZTD differences between pairs of techniques during CONT campaigns and the mean of the standard deviations over all sites contributing to a CONT campaign (see Table 8).

The standard deviations between GNSS and VLBI ZTD series at Ny-Ålesund (NYA1) are similar for all CONT campaigns and smaller than 4 mm. This is due to the low humidity

Table 8 Biases and standard deviations of the ZTD differences in mm between GNSS and the other techniques for the co-located sites during CONT campaigns

Techniques	CONT Camp.	Ny-Ålesund	Onsala	Wettzell	Westford	Tsukuba	Kokee Park	Hartebeesthoek	TIGO Concepcion
GNSS-VLBI	CONT02	−0.8 (3.5) (0.99)	−1.4 (4.2) (0.98)	−0.7 (4.8) (0.98)	5.1 (4.9) (0.99)	–	0.3 (9.7) (0.98)	−2.2 (7.7) (0.98)	–
	CONT05	−0.3 (3.0) (0.99)	−1.7 (4.9) (0.99)	−0.2 (5.0) (0.99)	6.9 (8.1) (0.99)	−3.4 (8.3) (0.99)	−2.2 (11.2) (0.96)	−3.0 (6.7) (0.92)	0.5 (6.0) (0.98)
	CONT08	0.8 (3.2) (1.00)	−2.4 (4.5) (0.99)	−0.6 (4.7) (0.99)	6.5 (6.0) (0.99)	−0.1 (11.5) (0.98)	−1.2 (9.3) (0.94)	0.6 (5.2) (0.99)	4.1 (5.9) (0.99)
	CONT11	1.4 (4.0) (0.98)	−1.3 (5.4) (0.99)	2.2 (4.2) (0.99)	6.2 (5.5) (1.00)	−2.9 (9.0) (0.99)	0.1 (8.5) (0.96)	1.1 (7.3) (0.98)	1.7 (5.2) (0.99)
GNSS-DORIS	CONT02	5.7 (7.9) (0.97)	–	–	–	–	−4.5 (44.7) (0.77)	−0.5 (14.4) (0.93)	–
	CONT05	5.4 (5.3) (0.96)	–	–	–	–	4.4 (8.8) (0.97)	2.8 (9.6) (0.88)	–
	CONT08	1.6 (4.4) (0.99)	–	–	–	–	−0.2 (9.7) (0.92)	−1.6 (17.3) (0.89)	–
	CONT11	0.6 (4.7) (0.98)	–	–	–	–	−2.1 (10.5) (0.94)	5.7 (10.9) (0.94)	–
GNSS-WVR	CONT02	–	−4.4 (7.2) (0.94)	−17.4 (7.7) (0.97)	–	–	−9.8 (8.1) (0.95)	–	–
	CONT05	–	0.9 (4.5) (0.99)	−9.9 (5.2) (0.99)	–	−27.5 (10.7) (0.98)	−1.9 (6.1) (0.99)	−2.9 (8.8) (0.86)	–
	CONT08	–	−2.2 (3.8) (0.99)	−14.1 (7.5) (0.99)	–	−29.8 (8.7) (0.99)	–	–	–
	CONT11	–	−4.6 (4.1) (0.99)	–	–	−23.2 (6.9) (0.99)	–	–	–
GNSS-ECMWF	CONT02	−6.5 (5.6) (0.99)	0.3 (6.7) (0.94)	1.0 (10.5) (0.92)	−15.2 (10.3) (0.95)	–	−7.2 (18.8) (0.93)	−13.3 (19.4) (0.88)	–
	CONT05	−4.2 (4.0) (0.98)	−7.4 (11.3) (0.96)	−11.9 (12.7) (0.94)	2.9 (14.6) (0.98)	−13.1 (20.5) (0.93)	−3.9 (16.7) (0.90)	−21.1 (16.5) (0.72)	–4.4 (11.5) (0.92)
	CONT08	−2.1 (5.8) (0.99)	0.0 (10.9) (0.91)	−2.9 (12.1) (0.93)	0.6 (15.0) (0.92)	1.7 (21.6) (0.93)	3.2 (16.8) (0.79)	4.2 (8.3) (0.97)	3.6 (9.6) (0.96)
	CONT11	1.6 (7.2) (0.95)	−2.0 (10.3) (0.97)	2.7 (10.8) (0.92)	3.8 (16.7) (0.97)	−1.0 (18.7) (0.97)	5.6 (19.0) (0.81)	12.9 (14.0) (0.91)	3.7 (12.0) (0.93)
GNSS-HIRLAM	CONT02	–	−10.4 (8.6) (0.90)	−17.2 (10.1) (0.92)	–	–	–	–	–
	CONT05	–	−16.6 (12.6) (0.96)	−28.7 (13.8) (0.92)	–	–	–	–	–
	CONT08	–	−5.3 (17.0) (0.78)	−10.8 (9.9) (0.95)	–	–	–	–	–
	CONT11	4.5 (6.4) (0.96)	−9.2 (10.7) (0.96)	−4.8 (9.4) (0.94)	–	–	–	–	–
GNSS-MANAL	CONT05	–	–	–	–	−6.8 (19.9) (0.94)	–	–	–
	CONT11	–	–	–	–	3.1 (10.9) (0.99)	–	–	–
GNSS-CReSS	CONT08	–	–	–	–	5.8 (18.7) (0.94)	–	–	–

The ZHD calculated from surface pressure at VLBI stations were added to the ZWD of WVR. The standard deviations and Pearson correlation coefficients between the troposphere ZTD are written in brackets. All correlation coefficients are statistically significant (p values < 0.05)

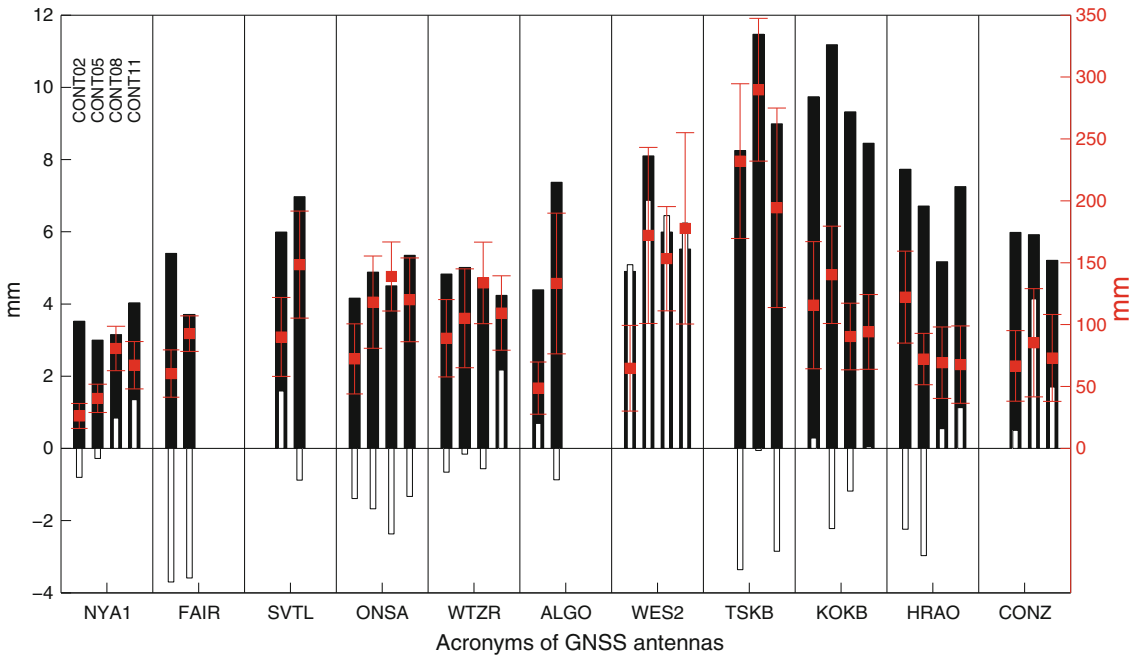

Fig. 4 Standard deviations (*black bars*) and biases (*white bars*) of the ZTD differences between GNSS and VLBI by station and CONT campaign. Mean ZWD and their standard deviations are shown in red. Only GNSS antennas participating in at least two CONT campaigns are included in this figure. The comparisons for all other stations are provided in the supplementary material

at Ny-Ålesund where the mean ZWD are below 8 cm for all CONT campaigns (see Figs. 4, 5). At Onsala (ONSA) and Wettzell (WTZR), the standard deviations are 4.2–5.4 mm, whereas at Tsukuba (TSKB) and Kokee Park (KOKB) the standard deviations are larger than 8 mm. This is due to the higher humidity at Tsukuba and Kokee Park compared to Ny-Ålesund, Onsala, and Wettzell (see Fig. 5). Except for Westford, the biases of ZTD between GNSS and VLBI vary between −3.4 and 4.1 mm over all sites and CONT campaigns. The biases at Onsala are negative at about −2 mm during all CONT campaigns (see Fig. 4; Table 8). Steigenberger et al. (2007) report similar ZWD biases (and standard deviations) between GNSS and VLBI with the values of −1.4 (4.2) mm at Ny-Ålesund (NYA1), −3.5 (5.3) mm at Onsala (ONSA), −1.1 (4.6) mm at Wettzell (WTZR) and −2.0 (8.1) mm at Tsukuba (TSKB). Ning et al. (2012) also found a similar bias and standard deviation between GPS and VLBI of −3.4 (5.1) mm at Onsala. However, Behrend et al. (2002) reported larger biases between GPS and VLBI of 3.9 mm at Onsala and 9.0 mm at Wettzell where the standard deviations are 5.7 and 7.4 mm, respectively.

The best ZTD agreement with the smallest standard deviation was found for Ny-Ålesund (NYA1) during CONT05 between GNSS and VLBI of 3 mm and between GNSS and ECMWF of 4 mm (see Table 8). The worst ZTD agreement between GNSS and VLBI is seen at Tsukuba (TSKB) during CONT08 with a standard deviation of 11.5 mm and at Kokee Park (KOKB) during CONT05 with a standard deviation of 11.2 mm. The largest standard deviations between GNSS and ECMWF are found at Tsukuba where the values are 20.5, 21.6, and 18.7 mm for CONT05, CONT08, and CONT11, respectively (see Table 8).

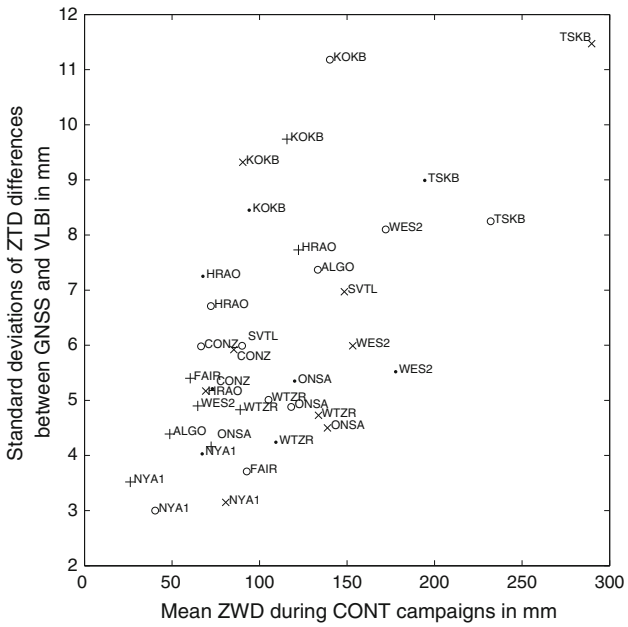

Fig. 5 Standard deviations of ZTD differences between GNSS and VLBI versus mean ZWD during CONT campaigns. The *plus* markers are for the CONT02 campaign, *circles* for CONT05, *crosses* for CONT08, and *dots* for CONT11

At Westford (WES2), we found large positive ZTD biases between GNSS and VLBI during all CONT campaigns, ranging from 5.1–6.9 mm. Snajdrova et al. (2006) and Steigenberger et al. (2007) found similar large positive biases between GNSS and VLBI at Westford (WES2) with 6.5 and 4.2 mm, respectively.

At most of the sites and for most CONT campaigns, the standard deviations between ZTD from GNSS and ECMWF is smaller by about 1–2 mm than those between VLBI and ECMWF and approximately 1.2–2 times larger than those between GNSS and VLBI (for details see supplementary material). Almost no reduction of standard deviations and biases between GNSS and VLBI is detected over CONT campaigns, as we would expect from e.g., the increased number of VLBI observations. An improvement by about 2.5 mm in standard deviation between VLBI and GNSS from CONT05 to CONT11 is found at Kokee Park (KOKB) and Westford (WES2). However, the opposite situation occurs at Svetloe (SVTL), Onsala (ONSA), and Algonquin Park (ALGO) where the standard deviation increases by about 1–2 mm over the CONT campaigns. Thus, we can hardly infer if there is an improvement of the agreement of ZTD between GNSS and VLBI over time comparing the CONT campaigns. On the other hand, the black bars and the red error bars in Fig. 4 show that the ZTD agreement between GNSS and VLBI techniques at a site depends mainly on the mean ZWD (see also Fig. 5) and the variation of ZWD (standard deviation of ZWD) over a campaign. This correlation between the agreement and the amount of ZWD and its variability during a CONT campaign is also valid for comparisons with ECMWF, which suggests that the humidity is the limiting factor for the level of agreement. Figure 5 shows the clear dependence of standard deviations of the ZTD differences between GNSS and VLBI on mean ZWD (amount of humidity) for CONT campaigns at co-located sites. Roughly speaking and considering all sites in the plot, the standard deviation increases by about 3 mm per 1 dm mean ZWD. For individual sites, this trend is not that obvious in Fig. 5.

The biases of ZTD between GNSS and ECMWF vary mostly between −15 and 5 mm over all CONT campaigns at all sites, except at Hartebeesthoek and at Fortaleza. The very similar situation is also valid between VLBI and ECMWF in terms of biases. Interested readers are referred to the supplementary material for the standard deviations of ZTD at each site, for each pair of techniques, and for each CONT campaign.

The best inter-technique agreement between GNSS and DORIS (similar to VLBI and DORIS) was found at Ny-Ålesund (NYA1-spjb) with standard deviations of 4.4 and 4.7 mm for CONT08 and CONT11, respectively. Teke et al. (2011) found a standard deviation of 5.4 mm between ZTD from GNSS and DORIS at Ny-Ålesund during CONT08, and Bock et al. (2010) found standard deviations between GNSS and DORIS at this site of about 5 mm (see supplementary plot of Bock et al. 2010). The positive biases between GNSS and DORIS at Ny-Ålesund decreased from 5.7 mm (CONT02) to 0.6 mm (CONT11) and between VLBI and DORIS from 6.8 mm (CONT02) to −0.6 mm (CONT11). At Kokee Park, the standard deviations between GNSS and DORIS (kokb) and between VLBI and DORIS are reduced from 44.7 and 41.1 mm (CONT02, koka) to 8.8 and 13.5 mm (CONT05, kolb). This is most likely due to the change of the DORIS beacon at this site from koka to kolb. The antenna koka was a first-generation DORIS beacon and not as accurate as the modern beacons. The standard deviations between VLBI and DORIS at Kokee Park (kolb) are 13.5, 12.1, and 12.0 mm during CONT05, CONT08, and CONT11, whereas GNSS and DORIS ZTD agreement is slightly better with 8.8, 9.7 and 10.5 mm, respectively. The agreement of ZTD between DORIS and the other space geodetic techniques, i.e., VLBI and GNSS, is best at Ny-Ålesund (spjb) with around 5 mm during CONT05, CONT08, and CONT11. However, this is not valid for KOKB-kolb where the standard deviations between GNSS and DORIS vary from 8.8 mm (CONT05) to 10.5 mm (CONT11) and for HRAO-hbmb where the standard deviations vary from 9.6 mm (CONT05) to 17.3 mm (CONT08) during the last three CONT campaigns. According to the bar plot of the supplementary material in Bock et al. (2010), they found that the standard deviation of ZTD between GNSS and DORIS is about 8 mm at Kokee Park (between KOKB and kolb) and about 11 mm at Hartebeesthoek (between HRAO and hbmb).

The standard deviations between ZTD from GNSS and WVR and from VLBI and WVR at co-located sites are in the order of 4–13 mm during the CONT campaigns. These results are in accordance with those derived by Behrend et al. (2002) at Onsala where the standard deviation is 6.9 mm between VLBI and WVR and 8.1 mm between GNSS (ONSA) and WVR. In our study, the standard deviations between GNSS and WVR do not reduce over CONT campaigns. The best agreement between ZTD from GNSS and WVR is at Onsala (ONSA), of which standard deviations vary between 3.8 mm (CONT08) and 7.2 mm (CONT02). During the last three CONT campaigns, large negative biases between GNSS (TSKB) and the WVR at Tsukuba are evident ranging from −23.2 mm (CONT11) to −27.5 mm (CONT05). (Note that there are similar large negative biases between VLBI and WVR at Tsukuba, see supplementary material of this paper.) Large negative biases for CONT02 (−17.4 mm), CONT05 (−9.9 mm), and CONT08 (−14.1 mm) are found at Wettzell between GNSS and WVR (WTZR). Snajdrova et al. (2006) and Teke et al. (2011) found very similar ZTD biases between GNSS (WTZR) and the WVR at Wettzell of about −14.7 mm for CONT02 and −12.5 mm for CONT08, respectively. The most likely sources of these large biases are WVR calibration errors at Wettzell and especially at Tsukuba. Since this

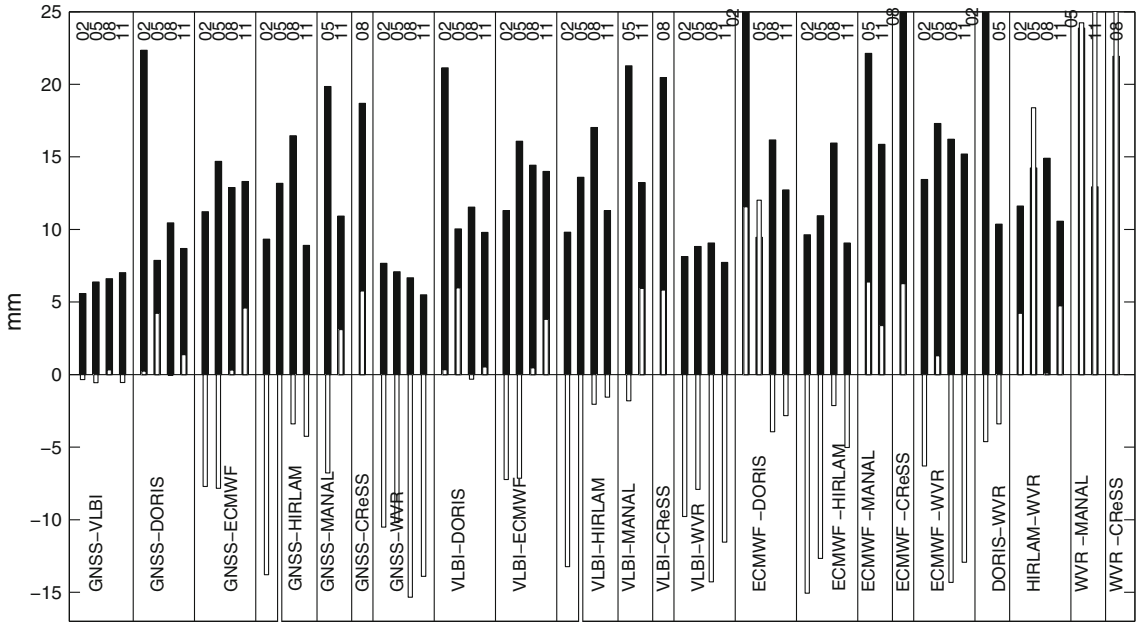

Fig. 6 Standard deviations (*black bars*) and biases (*white bars*) of ZTD differences over all stations in each CONT campaign

radiometer only measured in zenith it was not possible to perform a so-called tip-curve calibration (something which was regularly done at the other radiometers). Another possible reason could be errors in the conversion factors between brightness temperature and wet delay.

The agreement (standard deviation) between ECMWF and WVR does not improve over time at the co-located sites, varying from 9 mm (Onsala during CONT11) to 23.1 mm (Tsukuba during CONT08) during CONT campaigns. Large negative biases of −28.5 mm for CONT08 and −24.2 mm for CONT11 were found at Tsukuba. The best agreement of ZTD from HIRLAM with those derived from other techniques was found at Ny-Ålesund for CONT11 where the standard deviation e.g., w.r.t. GNSS (NYA1) is 6.4 mm, w.r.t. VLBI 6.8 mm, and w.r.t. ECMWF 5.0 mm. The agreement of ZTD from HIRLAM with GNSS, VLBI, and ECMWF at Onsala, Wettzell, and Zelenchukskaya varies between 8 and 17 mm. The standard deviations between GNSS and MANAL and between VLBI and MANAL (only at Tsukuba) are smaller by about 10 mm for CONT11 compared to CONT05. The standard deviations of MANAL w.r.t. VLBI and GNSS are 13.2 and 10.9 mm during CONT11.

Figure 6 depicts the mean standard deviations and biases of ZTD differences between each pair of techniques over all sites for the CONT campaigns. Over CONT campaigns, the mean standard deviations between GNSS and WVR steadily decrease from 7.7 mm (CONT02) to 5.5 mm (CONT11), whereas the mean standard deviations between GNSS and VLBI increase from 5.6 mm (CONT02) to 7.0 mm (CONT11). The higher mean standard deviation between ZTD from GNSS and VLBI for CONT11 is mostly due to the noisier VLBI data at Zelenchukskaya. If the data from this station are excluded from the analysis, the mean ZTD standard deviation between GNSS and VLBI for CONT11 decreases to 6.2 mm (see the plot of ZTD estimates from different techniques at Zelenchukskaya during CONT11, provided in supplementary material). After CONT02, the mean ZTD standard deviations between DORIS and GNSS decrease from 22.4 to 7.9 mm, between DORIS and VLBI from 21.1 to 10.0 mm, and between DORIS and ECMWF from 33.1 to 9.5 mm, mostly due to the improvement of DORIS at Kokee Park.

We found that the agreement within the space geodetic techniques is significantly better than with the NWM. The mean standard deviations of ECMWF w.r.t. space geodetic techniques during the last three CONT campaigns are not reduced and vary between 10 and 15 mm. In terms of mean standard deviations of ZTD, the agreement of DORIS and MANAL with other techniques improves over the CONT campaigns. Except for the aforementioned techniques, mean standard deviations of ZTD between any pair of techniques do not decrease over CONT campaigns. The mean standard deviations of ZTD between ECMWF and HIRLAM are 9.6 mm for CONT02, 10.9 mm for CONT05, 16.0 mm for CONT08, and 9.1 mm for CONT11. These agreements between ECMWF and HIRLAM are better compared to those between ECMWF and the other techniques for most of the CONT campaigns.

All correlations between ZTD are statistically significant at each site, for each technique, and CONT campaign. Most of the correlation coefficients of ZTD are above 0.95. However, the correlations of ZTD are weaker at Hartebeesthoek

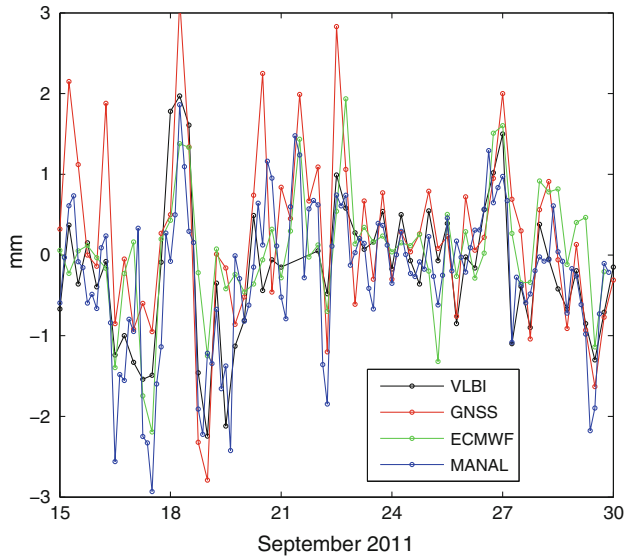

Fig. 7 Troposphere east gradients at the co-located site Tsukuba during CONT11. The GNSS antenna is TSKB

and Kokee Park than those at other sites between most of the techniques. For instance, at Hartebeesthoek the ZTD correlations between GNSS and DORIS are between 0.88 and 0.94, and between GNSS and ECMWF they range from 0.72 to 0.91 (see Table 8). Correlation coefficients between ECMWF and MANAL and between ECMWF and WVR at Tsukuba during CONT11 are 0.98 and 0.94, respectively (see supplementary material).

4.4 Inter-technique comparisons of troposphere gradients

In this section, site-wise inter-technique comparisons of troposphere east and north gradients are presented. As an example, Fig. 7 shows troposphere east gradients derived from different techniques at the co-located site Tsukuba during CONT11. Although the standard deviations between troposphere gradients from the different techniques at Tsukuba during CONT11 are rather large (on the order of 0.6–0.9 mm), most of the correlations are strong at about 0.7. Interested readers are referred to have a look at the supplementary files in which all the site-wise and mean standard deviations, biases, and correlations of troposphere east and north gradients between techniques for the CONT campaigns are provided.

For all CONT campaigns, the standard deviations of north and east gradient differences between GNSS and VLBI are largest at Zelenchukskaya (ZECK), Tsukuba (TSKB), Kokee Park (KOKB), and Hartebeesthoek (HRAO) with the values larger than 0.6 mm (e.g., see Fig. 8; Table 9, and supplementary material). Additionally, for these sites the standard deviations of north gradients are larger than for east gradients by 0.1–0.5 mm. Besides the above-mentioned sites, the standard deviations of east and north gradients between GNSS and ECMWF are larger at Westford (WES2) and Medicina (MEDI) with values above 0.6 mm. Teke et al. (2011) found similar results. However, standard deviations of gradient differences between GNSS and VLBI at co-located sites during CONT08 from this study are slightly smaller (by about 0.1–0.3 mm) and correlations are stronger than those derived by Teke et al. (2011). This is caused by the gradient estimation intervals of the studies. In this study gradients are estimated every 6 h for both GNSS and VLBI, while daily gradients of GNSS and 6 hourly VLBI gradients were compared at common epochs (at 0 UT) by Teke et al. (2011).

We found large positive north and east gradient biases between GNSS and VLBI and between GNSS and ECMWF at Westford (WES2) (from 0.3–0.7 mm) for all CONT campaigns. On the other hand, north gradient biases between VLBI and ECMWF are negative ranging from −0.1 to −0.4 mm for nearly all CONT campaigns and sites with the exceptions of Tsukuba and Hartebeesthoek during CONT08. At Kokee Park, the north and east gradient biases between GNSS and ECMWF are all negative with values from −0.2 to −0.5 mm (see Table 9 for east gradients and supplementary material for north gradients).

The best agreement of north and east gradients are seen at Ny-Ålesund between GNSS and VLBI for all CONT campaigns with a standard deviation of about 0.3 mm, biases of less than 0.1 mm, and strong correlations of 0.6–0.8. Similarly, the best agreement of gradients between GNSS and ECMWF is seen at Ny-Ålesund where the standard deviations of the differences are on the order of 0.2–0.4 mm, biases of about −0.2–0 mm, and correlations range from 0.5–0.7. Results (standard deviations, biases and correlations) between VLBI and ECMWF are very similar to those between GNSS and VLBI and between GNSS and ECMWF at Ny-Ålesund. The second best agreement of gradients between GNSS and VLBI is found for Wettzell (WTZR) and Onsala (ONSA). At both sites the standard deviations of north and east gradients are about 0.4 mm, the biases range from −1 to 1 mm, and correlations are in the order of 0.6–0.8. Comparisons between VLBI and ECMWF and between GNSS and ECMWF support these results; however, for these sites the standard deviations are slightly smaller between GNSS and ECMWF and between GNSS and VLBI than those between VLBI and ECMWF. Contrary to the differences between GNSS and VLBI, the north gradient differences between VLBI and ECMWF and between GNSS and ECMWF are negative for all CONT campaigns at Wettzell and Onsala (see supplementary material).

The worst agreement (largest standard deviations) of gradients between GNSS and VLBI is found at Zelenchukskaya, Kokee Park (KOKB), and Tsukuba (TSKB). The standard deviation of east gradient differences between GNSS and VLBI decreases at Kokee Park (KOKB) over the CONT

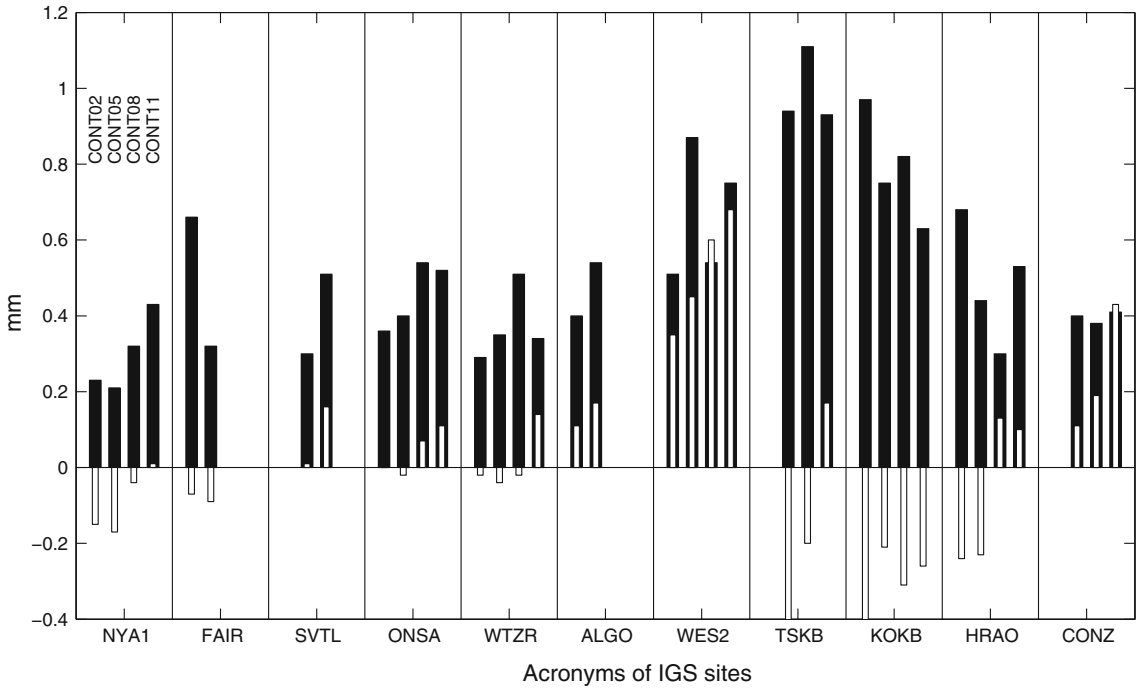

Fig. 8 Standard deviations (*black bars*) and biases (*white bars*) of the east gradient differences between GNSS and ECWMF per station and CONT campaign. Only GNSS antennas participating in at least two CONT campaigns are included in this figure. The comparisons for all other stations are provided in the supplementary material

campaigns from 0.9 mm (CONT02) to 0.6 mm (CONT11) and for north gradients from 1.4 mm (CONT05) to 0.6 mm (CONT11). The standard deviations between gradients from GNSS and VLBI at Hartebeesthoek (HRAO) are rather high at about 0.6–1 mm, except for CONT08.

The best agreement of gradients between GNSS and DORIS during the CONT campaigns is found at Ny-Ålesund (NYA1-spjb). This is due to a large number of sun-synchronous (hence with almost polar orbit) DORIS satellites passes at the station in the far north as discussed in Le Bail (2006), and Williams and Willis (2006) when analyzing station positioning results. On the other hand, nearly all correlations at Ny-Ålesund, Kokee Park, and Hartebeesthoek for CONT campaigns are weak and insignificant (e.g., see Table 9). The statistical insignificance of correlations between DORIS gradients and the other techniques is in the first place due to having only 15 common epochs with the other techniques, which leads to a small value of degrees of freedom and statistical insignificance.

We calculated the mean over the site-wise standard deviations of troposphere east and north gradient differences between techniques and refer to them as mean standard deviation of troposphere gradients (see supplementary material). The best agreements of troposphere east gradients in terms of mean standard deviations are between VLBI and ECMWF, GNSS and ECMWF, GNSS and VLBI, and between ECMWF and MANAL with values of about 0.7 mm or less during CONT campaigns.

The mean standard deviations of north gradients are slightly larger than of east gradients and vary between 0.1–0.3 mm.The agreement of gradients from different techniques does not improve over CONT campaigns except for DORIS, WVR, and MANAL. For example, the mean standard deviations of east gradients between GNSS and DORIS decrease from 1.7 to 1.0 mm after CONT02.

5 Discussion and conclusions

We estimated ZTD and troposphere gradients from VLBI, GNSS, and DORIS during four continuous VLBI campaigns (CONT02, CONT05, CONT08, and CONT11) over 2 weeks at co-located sites. In the analyses of the measurements of these space geodetic techniques we used state-of-the-art software following identical processing options as closely as possible. We aimed at using consistent geophysical and geodetic models, and we also harmonized the time intervals for the estimation of troposphere parameters; however, the latter was not possible for DORIS due to the irregular distribution of satellite passes. The troposphere parameters from the space geodetic techniques were compared not only against each other, but also against values derived from numerical weather models and water vapor radiometers. We provided a rigorous comparison in terms of standard deviations, biases, and correlation coefficients, taking into account the height differences between the antennas. To account for rapid

Table 9 Biases and standard deviations of the troposphere east gradient differences in mm between GNSS and other techniques for the co-located sites during CONT campaigns

Techniques	CONT Camp.	Ny-Ålesund	Onsala	Wettzell	Westford	Tsukuba	Kokee Park	Hartebeesthoek	TIGO Concepcion
GNSS-VLBI	CONT02	−0.1 (0.3) (0.46)	−0.1 (0.4) (0.58)	−0.1 (0.4) (0.69)	0.4 (0.4) (0.75)	–	−0.5 (0.9) (0.40)	−0.5 (0.8) (0.28)	–
	CONT05	0.0 (0.2) (0.67)	−0.1 (0.4) (0.81)	−0.1 (0.4) (0.67)	0.5 (1.0) (0.39)	−0.3 (1.0) (0.57)	−0.1 (0.9) (0.45)	−0.2 (0.6) (**0.09**)	−0.1 (0.6) (0.50)
	CONT08	0.0 (0.3) (0.75)	0.1 (0.4) (0.84)	0.0 (0.5) (0.69)	0.6 (0.5) (0.82)	0.2 (1.1) (0.60)	−0.1 (0.9) (0.40)	0.1 (0.5) (0.27)	−0.1 (0.5) (0.64)
	CONT11	0.1 (0.3) (0.84)	0.2 (0.4) (0.76)	0.1 (0.4) (0.71)	0.5 (0.5) (0.75)	0.4 (0.8) (0.72)	−0.4 (0.6) (0.65)	0.2 (0.7) (**0.23**)	0.4 (0.5) (0.57)
GNSS-DORIS	CONT02	0.5 (0.6) (**0.23**)	–	–	–	–	−1.1 (2.4) (**0.02**)	−0.5 (1.2) (**0.14**)	–
	CONT05	0.3 (0.4) (**0.37**)	–	–	–	–	0.4 (1.2) (**0.07**)	0.6 (0.5) (**0.59**)	–
	CONT08	0.3 (0.5) (−**0.03**)	–	–	–	–	−0.9 (1.1) (**0.23**)	−0.5 (0.8) (**0.06**)	–
	CONT11	0.3 (0.7) (**0.22**)	–	–	–	–	−0.4 (0.8) (**0.51**)	−0.2 (1.2) (−0.73)	–
GNSS-WVR	CONT02	–	0.1 (0.5) (0.36)	−0.4 (1.9) (**0.00**)	–	–	−1.2 (1.8) (**0.17**)	–	–
	CONT05	–	–	0.0 (0.4) (0.79)	–	–	−0.4 (1.2) (0.53)	−0.3 (0.5) (0.35)	–
	CONT08	–	0.4 (0.4) (0.88)	0.1 (0.4) (0.78)	–	–	–	–	–
	CONT11	–	0.2 (0.5) (0.62)	–	–	–	–	–	–
GNSS-ECMWF	CONT02	−0.2 (0.2) (0.59)	0.0 (0.4) (0.55)	0.0 (0.3) (0.66)	0.4 (0.5) (0.64)	–	−0.5 (1.0) (0.28)	−0.2 (0.7) (**0.20**)	–
	CONT05	−0.2 (0.2) (0.65)	0.0 (0.4) (0.63)	0.0 (0.4) (0.59)	0.5 (0.9) (0.53)	−0.6 (0.9) (0.56)	−0.2 (0.8) (0.47)	−0.2 (0.4) (0.50)	0.1 (0.4) (0.60)
	CONT08	0.0 (0.3) (0.66)	0.1 (0.5) (0.71)	0.0 (0.5) (0.56)	0.6 (0.5) (0.76)	−0.2 (1.1) (0.52)	-0.3 (0.8) (**0.17**)	0.1 (0.3) (**0.23**)	0.2 (0.4) (0.59)
	CONT11	0.0 (0.4) (0.53)	0.1 (0.5) (0.51)	0.1 (0.3) (0.64)	0.7 (0.8) (0.36)	0.2 (0.9) (0.57)	-0.3 (0.6) (**0.19**)	0.1 (0.5) (**0.15**)	0.4 (0.4) (0.55)
GNSS-MANAL	CONT05	–	–	–	–	−0.3 (1.1) (0.42)	–	–	–
	CONT11	–	–	–	–	0.5 (0.8) (0.69)	–	–	–
GNSS-CReSS	CONT08	–	–	–	–	0.2 (1.2) (0.42)	–	–	–

All the gradients except those derived from WVR (wet gradients) are total gradients. The standard deviations and Pearson correlation coefficients between the troposphere east gradient time series are written in brackets where insignificant correlation coefficients (p values > 0.05) are styled as bold

variations of troposphere ties over short time intervals, we corrected ZTD at each estimation epoch, which leads to a more rigorous comparison than introducing a mean value per CONT campaign. Some results are shown in the paper, but all statistics and all plots are available as supplementary material.

VLBI CONT campaigns are intended to demonstrate the highest accuracy which VLBI is capable of at that time. Due to improved observation strategies, e.g., an increased number of VLBI observations, we would expect an improvement in the accuracy of the VLBI results. This should also be reflected in a better agreement of troposphere parameters, which should be essentially the same at co-located sites at the same time epochs. A similar improvement is expected for numerical weather models with an ever-increasing number of observations entering the modeling process. However, we do not find a significant improvement of the agreement of troposphere parameters over time, i.e., from CONT02 to CONT11. Possible improvements are masked by different troposphere conditions during the four CONT campaigns and thus are not revealed here. The standard deviations depend mainly on the amount of water vapor in the troposphere above the site.

The biases of ZTD between GNSS and VLBI sites vary between −4 and 4 mm over all sites and CONT campaigns, except Westford. At Westford (WES2) we found systematic large positive ZTD biases between GNSS and VLBI of about 5–7 mm, but this kind of systematic large biases is not seen between GNSS and ECMWF, and the biases between VLBI and ECMWF at this site are all negative with a large bias of −21 mm during CONT02 and with biases between −5 and −3 mm during other CONT campaigns. This might suggest a problem with VLBI at this site. However, there are also large positive biases in both north and east gradients between GNSS and VLBI at Westford, but no corresponding bias between VLBI and ECMWF. This might indicate a problem with GNSS. Niell et al. (2001) showed that the ZTD agreement of GNSS with VLBI and WVR strongly depends on the elevation cutoff angle applied in the GNSS analysis, indicating that there are problems with multipath or antenna phase centre variations at this site. More investigations are needed to precisely find the reason for these biases. Another peculiarity is the large standard deviation of 15.1 mm for ZTD between VLBI and GNSS (ZECK) at Zelenchukskaya for CONT11, which is due to noisier VLBI observations at this site. Large standard deviations were also found for troposphere gradient differences between VLBI and the other techniques co-located at this site.

Site-wise inter-technique comparisons for CONT campaigns clearly show that there is a distinct difference of standard deviations and biases of ZTD and gradients between certain stations, at least partly caused by the amount of humidity and its variability over time and space. For example, a better agreement of ZTD and gradients is found for Ny-Ålesund, Onsala, and Wettzell than for Tsukuba and Kokee over all CONT campaigns.

In future, with an increasing amount of troposphere parameters from space geodetic techniques assimilated in the NWM, the agreement between space geodetic techniques and NWM should benefit greatly. In turn, this will have a positive impact on the accuracy of space geodetic techniques, because e.g., mapping functions can then be derived more precisely from NWM.

Acknowledgments This work is supported by the Austrian Science Fund (FWF) project, P20902-N10 (GGOS Atmosphere). Kamil Teke acknowledges Scientific and Technological Research Council of Turkey (Tübitak) for the financial support of the postdoctoral research programme, 2219. The work of DORIS was supported by the Centre National d'Etudes Spatiales (CNES) and based on observations with DORIS embarked on SPOTs, TOPEX/Poseidon, Envisat, Jason-2 and Cryosat-2 satellites. This paper is IPGP-3403 contribution. We used in this study the data provided by the International VLBI Service for Geodesy and Astrometry (IVS, Schuh and Behrend 2012), the International GNSS Service (IGS, Dow et al. 2009), the International DORIS Service (IDS, Willis et al. 2010a), the Centre for Orbit Determination in Europe (CODE, Dach et al. 2009), the European Centre for Medium-Range Weather Forecast (ECMWF, Dee et al. 2011), the Japan Meteorological Agency (JMA, Saito et al. 2006), and the authors would like to thank all components of the aforementioned services. The authors want to acknowledge SMHI and AEMet for providing HIRLAM (Undén et al. 2002) data for different grid spacings for all CONT sessions.

References

Altamimi Z, Collilieux X, Métivier L (2011) ITRF2008: an improved solution of the international terrestrial reference frame. J Geod 85(8):457–473. doi:10.1007/s00190-011-0444-4

Behrend D, Cucurull L, Vila J, Haas R (2000) An inter-comparision study to estimate zenith wet delays using VLBI, GPS, and NWP models. Earth Planets Space 52:691–694

Behrend D, Haas R, Pino D, Gradinarsky LP, Keihm SJ, Schwarz W, Cucurull L, Rius A (2002) MM5 derived ZWDs compared to observational results from VLBI, GPS and WVR. Phys Chem Earth 27:3301–3308

Bevis M, Businger S, Herring TA, Rocken C, Anthes RA, Ware RH (1992) GPS Meteorology. Remote sensing of atmosphere water vapor using the Global Positioning System. J Geophys Res 97(D14):15787–15801. doi:10.1029/92JD01517

Bizouard C, Gambis D (2009) The combined solution C04 for Earth orientation parameters consistent with International Terrestrial Reference Frame. In: Drewes H (ed) Geodetic reference frames. IAG Symp, vol 134, pp 265–270. doi:10.1007/978-3-642-00860-3_41

Bock O, Willis P, Lacarra M, Bosser P (2010) An inter-comparison of zenith tropospheric delays derived from DORIS and GPS data. Adv Space Res 46(12):1648–1660. doi:10.1016/j.asr.2010.05.018

Böhm J, Schuh H (2007) Troposphere gradients from the ECMWF in VLBI analysis. J Geod 81(6–8):403–408. doi:10.1007/s00190-007-0144-2

Böhm J, Werl B, Schuh H (2006) Troposphere mapping functions for GPS and very long baseline interferometry from European Center for Medium-Range Weather Forecasts operational analysis data. J Geophys Res 111:B02406. doi:10.129/2005JB003629

Böhm J, Böhm S, Nilsson T, Pany A, Plank L, Spicakova H, Teke K, Schuh H (2012) The new Vienna VLBI Software VieVS. Geodesy

for Planet Earth. In: Kenyon S, Pacino MC, Marti U (eds) Proceedings of the 2009 IAG symp, Buenos Aires. International Association of Geodesy Symposia Series, vol 136, pp 1007–1011. doi:10.1007/978-3-642-20338-1_126 (2009)

Brunner FK, Rüeger JM (1992) Theory of the local scale parameter method for EDM. Bull Géodésique 66:355–364

Chen G, Herring TA (1997) Effects of atmospheric azimuthal asymmetry on the analysis from space geodetic data. J Geophys Res 102(B9):20489–20502. doi:10.1029/97JB01739

Cucurull L, Navascues B, Ruffini G, Elosegui P, Rius A, Vila J (2000) The use of GPS to validate NWP systems: the HIRLAM model. J Atmos Ocean Technol 17(6):773–787

Dach R, Hugentobler U, Fridez P, Meindl M (eds) (2007) Bernese GPS Software Version 5.0, Astronomical Institute, University of Bern

Dach R, Brockmann E, Schaer S, Beutler G, Meindl M, Prange L, Bock H, Jäggi A, Ostini L (2009) GNSS processing at CODE: status report. J Geod 83(3–4):353–365. doi:10.1007/s00190-008-0281-2

Dach R, Schaer S, Lutz S, Meindl M, Bock H, Orliac E, Prange L, Thaller D, Mervart L, Jäggi A, Beutler G, Brockmann E, Ineichen D, Wiget A, Weber G, Habrich H, Ihde J, Steigenberger P, Hugentobler U (2012) Center for Orbit Determination in Europe (CODE), In: Meindl M, Dach R, Jean Y (eds) International GNSS Service Technical Report 2011

Davis JL, Herring TA, Shapiro II (1991) Effects of atmospheric modeling errors on determinations of baseline vectors from VLBI. J Geophys Res 96(B1):643–650. doi:10.1029/90JB01503

Davis JL, Elgered G, Niell AE, Kuehn CE (1993) Ground-based measurements of gradients in the "wet" radio refractivity of air. Radio Sci 28(6):1003–1018. doi:10.1029/93RS01917

Davis JL, Herring TA, Shapiro II, Rogers AEE, Elgered G (1985) Geodesy by radio interferometry: effects of atmospheric modeling errors on estimates of baseline length. Radio Sci 20(6):1593–1607. doi:10.1029/RS020i006p01593

Dee D, Uppala S, Simmons A, Berrisford P, Poli P, Kobayashi S, Andrae U, Balmaseda M, Balsamo G, Bauer P, Bechtold P, Beljaars A, van de Berg L, Bidlot J, Bormann N, Delsol C, Dragani R, Fuentes M, Geer A, Haimberger L, Healy S, Hersbach H, Holm E, Isaksen L, Kallberg P, Köhler M, Matricardi M, McNally T, Monge-Sanz B, Morcrette JJ, Park BK, Peubey C, de Rosnay P, Tavolato C, Thépaut JN, Vitart F (2011) The ERA-Interim reanalysis: configuration and performance of the data assimilation system. Q J R Meteorol Soc 137:553–597. doi:10.1002/qj.828

Dow JM, Neilan RE, Rizos C (2009) The International GNSS Service in a changing landscape of Global Navigation Satellite Systems. J Geod 83:191–198. doi:10.1007/s00190-008-0300-3

Elgered G (1993) Tropospheric radio path delay from ground-based microwave radiometry. In: Janssen M (ed) Atmospheric remote sensing by microwave radiometry. Wiley, New York, pp 215–258

Elgered G, Jarlemark POJ (1998) Ground-based microwave radiometry and long term observations of atmospheric water vapor. Radio Sci 33(3):707–717. doi:10.1029/98RS00488

Fey A, Gordon D, Jacobs CS (2009) The second realization of the International Celestial Reference Frame by very long baseline interferometry. IERS Technical Note, vol 35. Verlag des Bundesamts für Kartographie und Geodäsie, Frankfurt am Main, ISBN 3-89888-918-6

Gradinarsky LP, Haas R, Elgered G, Johansson JM (2000) Wet path delay and delay gradients inferred from microwave radiometer, GPS and VLBI observations. Earth Planets Space 52(10):695–698

Gobinddass ML, Willis P, Menvielle M, Diament M (2010) Refining DORIS atmospheric drag estimation in preparation of ITRF2008, in DORIS special issue: precise orbit determination and applications to the Earth sciences, Willis P (ed). Adv Space Res 46(12):1566–1577. doi:10.1016/j.asr.2010.04.004

Gobinddass ML, Willis P, Sibthorpe AJ, Zelensky NP, Lemoine FG, Ries JC, Ferland R, Bar-Sever YE, de Viron O, Diament M (2009) Improving DORIS geocenter time series using an empirical rescaling of solar radiation pressure models. Adv Space Res 44(11):1279–1287. doi:10.1016/j.asr.2009.08.004

Heinkelmann R, Böhm J, Bolotin S, Engelhardt G, Haas R, Lanotte R, MacMillan DS, Negusini M, Skurikhina E, Titov O, Schuh H (2011) VLBI-derived troposphere parameters during CONT08. J Geod 85(7):377–393. doi:10.1007/s00190-011-0459-x

Herring TA (1986) Precision of vertical estimates from very long baseline interferometry. J Geophys Res 91(B9):9177–9182. doi:10.1029/JB091iB09p09177

Hobiger T, Ichikawa R, Koyama Y, Kondo T (2008a) Fast and accurate ray-tracing algorithms for real-time space geodetic applications using numerical weather models. J Geophys Res 113:D20302. doi:10.1029/2008JD010503

Hobiger T, Ichikawa R, Takasu T, Koyama Y, Kondo T (2008b) Ray-traced troposphere slant delays for precise point positioning. Earth Planets Space 60(5):e1–e4

Hobiger T, Shimada S, Shimizu S, Ichikawa R, Koyama Y, Kondo T (2010) Improving GPS positioning estimates during extreme weather situations by the help of fine-mesh numerical weather models. J Atmos Solar Terr Phys 72(2–3):262–270. doi:10.1016/j.jastp.2009.11.018

Jarlemark P (1997) Analysis of temporal and spatial variations in atmospheric water vapor using microwave radiometry, PhD Thesis, Technical Report 308, School of Electrical Engineering, Chalmers University of Technology, Göteborg

Le Bail K (2006) Estimating the noise in space-geodetic positioning: the case of DORIS. J Geod 80(8–11):541–565. doi:10.1007/s00190-006-0088-y

Lyard F, Lefevre F, Lettelier T, Francis O (2006) Modelling the global ocean tides, Modern insights from FES2004. Ocean Dyn 56(6):394–415. doi:10.1007/s10236-006-0086-x

MacMillan DS, Ma C (1994) Evaluation of very long baseline interferometry atmospheric modeling improvements. J Geophys Res 99(B1):637–651. doi:10.1029/93JB02162

MacMillan DS, Ma C (1997) Atmospheric gradients and the VLBI terrestrial and celestial reference frames. Geophys Res Lett 24(4):453–456. doi:10.1029/97GL00143

Nafisi V, Urquhart L, Santos M, Nievinski F, Böhm J, Wijaya D, Schuh H, Ardalan A, Hobiger T, Ichikawa R, Zus F, Wickert J, Gegout P (2012) Comparison of ray-tracing packages for troposphere delays. IEEE Trans Geosci Remote Sens 50(2):469–481

Niell AE, Coster AJ, Solheim FS, Mendes VB, Toor PC, Langley RB, Upham CA (2001) Comparison of measurements of atmospheric wet delay by radiosonde, water vapor radiometer, GPS, and VLBI. J Atmos Ocean Technol 18:830–850

Ning T, Haas R, Elgered G, Willén U (2012) Multi-technique comparisons of 10 years of wet delay estimates on the west coast of Sweden. J Geod 86(7):565–575. doi:10.1007/s00190-011-0527-2

Petit G, Luzum B (2010) IERS conventions 2010, IERS Technical Note; 36. Verlag des Bundesamts für Kartographie und Geodäsie, Frankfurt am Main., ISBN 3-89888-989-6

Petrov L, Boy JP (2004) Study of the atmospheric pressure loading signal in very long baseline Interferometry observations. J Geophys Res 109(B3):B03405. doi:10.1029/2003JB002500

Rebischung P, Griffiths J, Ray J, Schmid R, Collilieux X, Garayt B (2012) IGS08: the IGS realization of ITRF2008. GPS Solut 16(4):483–494. doi:10.1007/s10291-011-0248-2

Rummel R, Rothacher M, Beutler G (2005) Integrated Global Geodetic Observing System (IGGOS)-science rationale. J Geodyn 40(4–5):357–362. doi:10.1016/j.jog.2005.06.003

Saastamoinen J (1972) Atmospheric correction for the troposphere and stratosphere in radio ranging of satellites. The use of artificial satellites for geodesy. Geophys Monogr Ser 15:274–251

Saito K, Fujita T, Yamada Y, Ishida JI, Kumagai Y, Aranami K, Ohmori S, Nagasawa R, Kumagai S, Muroi C, Kato T, Eito H, Yamazaki Y

(2006) The operational JMA nonhydrostatic mesoscale model. Mon Weather Rev 134:1266–1298

Schuh H, Behrend D (2012) VLBI: a fascinating technique for geodesy and astrometry. J Geodyn 61:68–80. doi:10.1016/j.jog.2012.07.007

Schervish MJ (1996) P values: what they are and what they are not. Am Stat 50(3):203–206. doi:10.2307/2684655

Snajdrova K, Böhm J, Willis P, Haas R, Schuh H (2006) Multi-technique comparison of tropospheric zenith delays derived during the CONT02 campaign. J Geod 79(10–11):613–623. doi:10.1007/s00190-005-0010-z

Steigenberger P, Tesmer V, Krügel M, Thaller D, Schmid R, Vey S, Rothacher M (2007) Comparisons of homogeneously reprocessed GPS and VLBI long time-series of troposphere zenith delays and gradients. J Geod 81(6–8):503–514. doi:10.1007/s00190-006-0124-y

Steigenberger P, Böhm J, Tesmer V (2009) Comparison of GMF/GPT with VMF1/ECMWF and implications for atmospheric loading. J Geod 83:943–951. doi:10.1007/s00190-009-0311-8

Steigenberger P, Hugentobler U, Lutz S, Dach R (2011) CODE contribution to the IGS reprocessing. Technical Report, Institut für Astronomische und Physikalische Geodäsie, TU München

Stoew B, Rieck C (1999) Dual channel water vapour radiometer development. In: Schlüter W, Hase H (eds) Proceedings of the 13th working meeting on European VLBI for geodesy and astrometry. Bundesamt für Kartographie und Geodäsie, Wettzell

Teke K, Böhm J, Nilsson T, Schuh H, Steigenberger P, Dach R, Heinkelmann R, Willis P, Haas R, Garcia-Espada S, Hobiger T, Ichikawa R, Shimizu S (2011) Multi-technique comparison of troposphere zenith delays and gradients during CONT08. J Geod 85(7):395–413. doi:10.1007/s00190-010-0434-y

Tesmer V, Boehm J, Heinkelmann R, Schuh H (2007) Effect of different tropospheric mapping functions on the TRF, CRF and position time-series estimated from VLBI. J Geod 81(6–8):409–421. doi:10.2007/s00190-006-0126-9

Tsuboki K, Sakakibara A (2002) Large-scale parallel computing of cloud resolving storm simulator. High Performance Computing, Springer, Berlin, pp 243–259. doi:10.1007/3-540-47847-7_21

Undén P, Rontu L, Järvinen H, Lynch P, Calvo J, Cats G, Cuxart J, Eerola K, Fortelius C, Garcia-Moya J A, Jones C, Lenderlink G, McDonald A, McGrath R, Navascues B, Woetman Nielsen N, Ødegaard V, Rodriguez E, Rummukainen M, Rõõm R, Sattler K, Hansen Sass B, Savijärvi H, Wichers Schreur B, Sigg R, The H, Tijm A (2002) HIRLAM-5 scientific documentation, Swedish Meteorological and Hyrdological Institute, Norrköping

Urquhart L, Nievinski FG, Santos MC (2011) Ray traced slant factors for mitigating the tropospheric delay at the observation level. J Geod 86(2):149–160. doi:10.1007/s00190-011-0503-x

Wijaya D, Böhm J, Karbon M, Schuh H (2013) Atmospheric pressure loading, In: Böhm J, Schuh H (eds) Atmospheric effects in space geodesy. Springer, Berlin, pp 137–157. doi:10.1007/978-3-642-36932-2_4

Williams SDP, Willis P (2006) Error analysis of weekly station coordinates in the DORIS network. J Geod 80(8–11):525–539. doi:10.1007/s00190-006-0056-6

Willis P, Ries JC, Zelensky NP, Soudarin L, Fagard H, Pavlis EC, Lemoine FG (2009) DPOD2005: an extension of ITRF2005 for precise orbit determination. Adv Space Res 44(5):535–544. doi:10.1016/j.asr.2009.04.018

Willis P, Fagard H, Ferrage P, Lemoine FG, Noll CE, Noomen R, Otten M, Ries JC, Rothacher M, Soudarin L, Tavernier G, Valette JJ (2010a) The International DORIS Service. Toward maturity. Adv Space Res 45(12):1408–1420. doi:10.1016/j.asr.2009.11.018

Willis P, Boucher C, Fagard H, Garayt B, Gobinddass ML (2010b) Contributions of the French Institut Geographique National (IGN) to the International DORIS Service. Adv Space Res 45(12):1470–1480. doi:10.1016/j.asr.2009.09.019

Willis P, Bar-Sever YE, Bock O (2012a) Estimating horizontal tropospheric gradients in DORIS data processing, preliminary results. IAG Symp 136:1013–1019. doi:10.1007/978-3-642-20338-1_127

Willis P, Gobinddass ML, Garayt B, Fagard H (2012b) Recent improvements in DORIS data processing in view of ITRF2008, the ignwd08 solution. IAG Symp 136:43–49. doi:10.1007/978-3-642-20338-1_6

Yang X, Sass BH, Elgered G, Johansson JM, Emardson TR (1999) A comparison of precipitable water vapor estimates by an NWP simulation and GPS observations. J Appl Meteorol 38:941–956